This is an open access article published under an ACS AuthorChoice License, which permits copying and redistribution of the article or any adaptations for non-commercial purposes.

ACS OMEGA

Article

Cite This: ACS Omega 2018, 3, 8567−8582

http://pubs.acs.org/journal/acsodf

Hydrophilic Ionic Liquid Mixtures of Weakly and Strongly Coordinating Anions with and without Water

Roberto Macchieraldo,[†] Lars Esser,[†] Roman Elfgen,[†,‡] Pascal Voepel,[§] Stefan Zahn,[∥] Bernd M. Smarsly,[§] and Barbara Kirchner*[,†]

[†]Mulliken Center for Theoretical Chemistry, University of Bonn, Beringstr. 4+6, D-53115 Bonn, Germany

[‡]Max Planck Institute for Chemical Energy Conversion, Stiftstr. 34-36, D-45413 Mülheim an der Ruhr, Germany

[§]Institute of Physical Chemistry and Center for Materials Research (LaMa), Justus-Liebig-University Giessen, Heinrich-Buff Ring 17+16, D-35392 Giessen, Germany

[∥]Leibniz Institute of Surface Engineering, Permoserstr. 15, D-04318 Leipzig, Germany

Supporting Information

ABSTRACT: With the aid of ab initio molecular dynamics simulations, we investigate an ionic liquid (IL) mixture composed of three components 1-butyl-3-methylimidazolium $[C_4C_1Im]^+$, tetrafluoroborate $[BF_4]^-$, and chloride $[Cl]^-$ without and with water. In the pure IL mixture, we observe an already complex network of interactions between cations and anions, and addition of water to the system even extends the complexity. Observed number integrals show that the coordination number between cations and anions is reduced in the system with water compared to that in the pure system. Further studies show that the Coulombic network of the strongly coordinating anion $[Cl]^-$ is disturbed by water, while that of the weakly coordinating anion $[BF_4]^-$ is not. These observations can also be confirmed by the Voronoi polyhedra analysis, which shows that the polar network of microheterogeneous IL collapses by the introduction of water. Hydrogen-acceptor interactions revealed that the $[Cl]^-$ anions are transferred from being situated in the IL to the water continuum, while $[BF_4]^-$ is almost unperturbed; these effects mainly influence the interplay of the ionic liquid network.

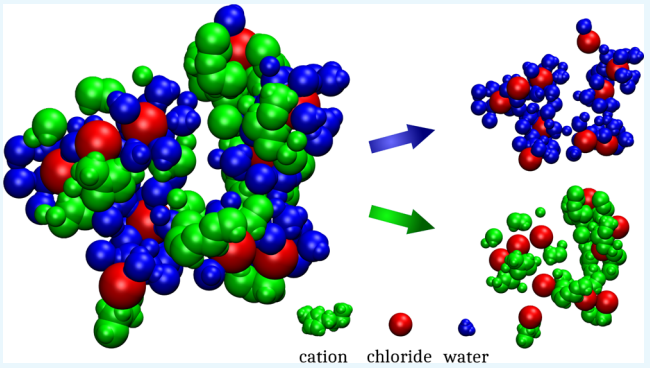

INTRODUCTION

Over the years ionic liquids (ILs) have gained distinct attraction for several purposes due to their unique characteristics. The applications range from being components of energy devices[1,2] like fuel cells[3] and electric double-layer capacitors[4−6] over to electrolytes in electrodeposition[7] or extractants.[8] ILs were investigated as reaction media for chemical processes, such as material synthesis, leading to alternative reaction paths or even to the formation of kinetically stabilized products, which could not be obtained otherwise.[9−15] Experimental approaches performed from the group of Balducci also show that ILs are promising candidates as electrolytes for supercapacitors to obtain high cycling stability and high stable capacitance.[16−21] Theoretical investigation on related subjects is carried out by Salanne and co-workers. They study for example the order obtained on the interface of ILs and electrochemical interfaces.[4,5,22−25] The knowledge obtained by using ILs in capacitors might lead to the viability of those as electrolytes for batteries under different conditions for the upcoming future.[19,26−29]

Due to the high variety of different cations and anions and the sheer amount of possible additional functionalizations, the combinations for ILs are immense,[30] showing a great opportunity, by simply modifying the properties of those for specific demands. However this task is nontrivial. In fact, the mere modification of an IL itself is not the only way to tune its properties, but the same result can be obtained by mixing the parent IL with molecular liquids or other ILs.[31−33]

In this regard, water represents the most common, accessible, and environmentally benign solvent. Therefore, a straightforward approach is to combine ILs with water, as diverse syntheses are based on the hydrolysis of metal compounds. Although the solubility of water in ILs is strongly dependent on the hydrophilicity/hydrophobicity of the IL, water is almost always present in ILs (e.g., impurities). It is known that even small amounts can influence the physicochemical properties of ILs significantly.[33−35] Consequently, many studies have been carried out to understand the influence of water on the properties of ionic liquids and also, conversely, by observing an altered reactivity of water in the presence of ILs.[36] For example,

Received: May 14, 2018
Accepted: July 20, 2018
Published: August 1, 2018

Downloaded via BONN LIBRARIES on November 12, 2020 at 15:00:43 (UTC).
See https://pubs.acs.org/sharingguidelines for options on how to legitimately share published articles.

© 2018 American Chemical Society

DOI: 10.1021/acsomega.8b00995
ACS Omega 2018, 3, 8567−8582

the reaction of water with phosphorus chlorides is prevented in imidazolium-based liquids, making these ILs unique media for phosphorous chemistry. Other examples consist of accurate thermodynamics studies on the uptake of water vapor and on the liquid−liquid equilibria.[34,37] Further studies also have shown that viscosity and density depend on the temperature and the water content of ILs.[38,39] Water was found to decrease the viscosity, while the overall density only slightly changed (1−2%).[38,39] Such studies made possible to recognize the reason for deviations between many experimental data, which was mainly due to the differences in the sample purities. Studies of solubility and miscibility[40,41] were also conducted and revealed that ILs can generally be subdivided into two groups: hydrophobic and hydrophilic ILs. Hydrophilic ILs, such as 1-ethyl-3-methylimidazolium bis(trifluoromethylsulfonyl)imide $[C_2C_1Im][NTf_2]$, possess anions with a low Lewis basicity, while hydrophilic ILs possess anions that can even abstract hydrogen atoms from imidazolium, such as 1-ethyl-3-methylimidazolium acetate $[C_2C_1Im][OAc]$. These specific properties make ILs uniquely suited for extraction processes. However, it must be individually selected which kind of IL group should be chosen.[42] In a recent work of Kohno and Ohno, this concept is evolved. ILs were successfully designed where the hydrophilic or hydrophobic behavior can be controlled reversibly by external criteria such as temperature. These IL/water mixtures can further be classified as upper critical solution temperature (UCST) phase transition and lower critical solution temperature (LCST) phase change mixtures. Mixtures of the UCST-type experience an increasing solubility between IL and water with rising temperature, whereas LCST types reverse these trends.[43] A main objective of many theoretical studies has been the observation of structural features such as the association behavior in general, the microphase segregation, and the hydrogen bond (HB) networks of IL/water mixtures. Through this kind of studies, we gain a deeper understanding at the molecular level of this class of substances, which then lead to a confirmed macroscopic characteristic of those obtained by experimental approaches.[33,44−51]However, these goals have also been pursued through experimental and even joint attempts.[45−47,52−57]

Such a joint approach was used by Raos et al. by combining molecular dynamics (MD) simulations and nuclear magnetic resonance (NMR) spectroscopy to describe the aggregation of water occurring in IL/water mixtures.[56] They identified two hydration regimes: The first was defined at low water contents, where water molecules strongly interact with both ions, disrupting the IL network. The second was defined at higher water contents, in which the interaction between water molecules and ions behaves nonselectively. This shows that most of the effects are due to the swelling of the water clusters. Canongia Lopes et al. extended these concepts based on an investigation of 1-ethyl-3-methylimidazolium ethylsulfate $[C_2C_1Im][C_2SO_4]$−water mixtures for which four structural regimes were observed:[48]

1. isolated water molecules ($x_{H_2O} < 0.5$)
2. chainlike water aggregates ($0.5 < x_{H_2O} < 0.8$)
3. bicontinuous system ($0.8 < x_{H_2O} < 0.95$)
4. isolated ions or small ion clusters ($x_{H_2O} > 0.95$)

This distinction includes two different percolation limits: that of water in the ionic liquid network ($x_{H_2O} \approx 0.8$) and that of the ionic liquid in water ($x_{H_2O} \approx 0.95$). However, it should also be noted that studies on dynamical properties are also made on the basis of theoretical and practical experiments. In this regard, it was observed that compared with the structuring and dynamics within the pure IL, the addition of water to $[C_2C_1Im][OAc]$ modifies and widely disturbs the dipole moment of the ions and the hydrogen bond network of the IL. Furthermore, it hinders a possible carbene formation, besides the fact that a free carbene is not likely.[33,58,59] Feng and Voth investigated the effect of the side chain length of the cation and the effect of the anion, for the IL−water mixtures of 1-butyl-3-methylimidazolium tetrafluoroborate ($[C_4C_1Im][BF_4]$), 1-octyl-3-methylimidazolium tetrafluoroborate ($[C_8C_1Im][BF_4]$), and 1-octyl-3-methylimidazolium chloride ($[C_8C_1Im][Cl]$) with water mole fractions ranging from 0.2 to 0.9615, on the mixture dynamics and structures.[51] While replacing $[C_4C_1Im]^+$ by $[C_8C_1Im]^+$ only leads to an increasing microheterogeneity due to a stronger agglomeration of the cations, exchanging $[BF_4]^-$ for $[Cl]^-$ results in a decrease in the diffusion due to stronger electrostatic interactions between $[Cl]^-$ and water as compared with the relatively weakly coordinating anion $[BF_4]^-$. It is stated that at low water concentrations the water structure within the mixtures depends on the strength of the water−anion interactions: In $[C_4C_1Im][BF_4]$ and $[C_8C_1Im][BF_4]$, formation of water clusters connected by hydrogen bonds is observed, which does not occur in $[C_8C_1Im][Cl]$. Further structural characterization of geminal dicationic and monocationic imidazolium-based ionic liquids with halides in mixtures with water was performed by D'Angelo et al. and Serva et al.[60,61] Extended X-ray absorption fine structure spectroscopy and MD simulations were combined to investigate IL−water mixtures ranging from 1:1 to 1:400. In all of these solutions, H_2O favored coordination to the halide ion. Although a complex interaction among cations, anions, and water occurred, ion pairing was still evidenced up to a ratio of 1:12. Even for the highly concentrated solutions, the existence of long-range structural correlations for the 1-hexyl-3-methylimidazolium iodide $[C_6C_1Im][I]$/water mixture was observed. It should also be noted that the local environment of the halides changes by increasing the water concentration, resulting in a growing accumulation of water molecules in the first solvent shell of the anions. Sharma and Ghorai examined the effect of water on the structure and dynamics of 1-butyl-3-methylimidazolium hexafluorophosphate ($[C_4C_1Im][PF_6]$) via all-atom MD simulations.[35] The study showed that the addition of water does not affect the number of dissociated ions compared to that in the pure state, which simultaneously results in similar self-diffusion coefficients for both the cation and the anion. However, Voronoi polyhedra analysis revealed a significant change of the ILs' local structure if water is present. Void and neck distributions in Voronoi tessellation showed that particularly for high water concentrations an increase in void space and neck size leads to a facilitation in ionic motion and therefore decreases dynamical heterogeneity and IL reorientation time, while increasing self-diffusion coefficients. Ludwig by means of a combined approach of Fourier-transform infrared spectroscopy and density functional theory (DFT) calculation has shown that water can be used as a sensitive probe for measuring the polarity of ionic liquids when other conventional methods fail. Using the same approach, he studied the structure and occurrence of ion-pair formation as a function of temperature and concentration. Furthermore, he investigated the influence of highly directional H-bonds, finding an opposite effect of the hydrogen bindings on ionic liquids. H-bonds can, in

DOI: 10.1021/acsomega.8b00995
ACS Omega 2018, 3, 8567−8582

fact, introduce "defects" into the Coulomb network, resulting in a fluidized ionic liquid.[62−70]

In this work, we continue the previous studies of binary ionic liquids interacting with water by investigating mixtures composed of $[C_4C_1Im]^+$, $[BF_4]^-$, and $[Cl]^-$ with water by ab initio molecular dynamics (AIMD) simulations. This mixture was recently used as a reaction medium to synthesize peculiar titanium oxide structures such as bronze-type TiO_2.[9] Therein, it was shown that the ratio of $[BF_4]^-$ and $[Cl]^-$ as well as the content of water had a significant impact on the formed crystal structure. However, before such a complex system is established, many variables must be considered. For instance, the choice of compositions is nontrivial because the individual component might be solid, leading to a heterogeneous system. For the pure IL system, we observe a very complex network of interactions between cations and anions, and addition of water to the system even extends the complexity. The motivation of this work is on the one hand to understand why this particular combination works so well for the different material synthesis[9−14] carried out in such systems. On the other hand, it is interesting to understand whether the combination of a weakly and strongly coordinating anion with water leads to such a powerful solvent system such as those obtained for binary mixtures by adding antagonistic salts,[71] i.e., systems in which cations and anions are preferentially dissolved in different microphases. This idea can be extended by selecting such ternary systems as extractants for heavy elements, like lanthanoids or actinoids, due to their capability of showing high resistance to strong oxidizing or reducing agents. For upcoming future projects, the evolved concept introduced by Kohno and Ohno, as discussed above,[43] might lead to other perspectives, taking into account UCST, LCST, or even addition of kosmotropic salts to ILs.

COMPUTATIONAL DETAILS

AIMD Simulations. To study the effect of water onto an ionic liquid mixture as it is applied in material synthesis,[9,10] the ionic liquid mixture composed of the three components $[C_4C_1Im]^+$, $[BF_4]^-$, and $[Cl]^-$ without and with water was chosen. We carried out AIMD simulations to discuss effects on the electronic structure level. This is not possible in force-field simulations because the intermolecular forces are fitted to reproduce some experimental quantities. Thus, our study allows the observation of specific interactions (in particular the differentiation between direct hydrogen atom contacts) that are unbiased in our simulation but only rely on the particular choice of electronic structure method. For example, the atomic specific interactions are obtained under explicit accounting of polarization. We can access the varying partial charges on the ions and atoms considering charge transfer and polarization effects, which are fixed in force-field simulations. Furthermore, we are able to calculate vibrational spectra. These are all quantities that are not or only poorly accessible in force-field simulations. Table 1 lists the number of components in system A and system B. The ratio among the number of components of $[C_4C_1Im]^+$, $[Cl]^-$, and $[BF_4]^-$ is the same for every system and is chosen according to the material synthesis.[9,10]

The initial configurations of the simulated cubic boxes were performed using PACKMOL, the chosen densities referred to the experimental values of the material synthesis mentioned before (e.g., Figure 1).[72] AIMD simulations have been performed using the CP2K[73] code and the built-in QUICKSTEP[74] module at a DFT approximation level. The QUICKSTEP method uses hybrid Gaussian and plane wave approaches

Table 1. Compositions of Simulated AIMD Systems Chosen According to Experimental Reaction Conditions of Refs 9, 10[a]

system	$[C_4C_1Im]^+$	$[Cl]^-$	$[BF_4]^-$	H_2O(w/w %)
A	32	10	22	0(0)
B	32	10	22	211(36)

[a]The numbers refer to the number of compounds in each system. For water, the mass percentage is shown in brackets.

to build the wave function and calculates the potential energy surface and the energy gradient acting on the atoms. The molecularly optimized double-ζ basis set (MOLOPT-DZVP-SR-GTH)[75] was chosen for all atoms with the revPBE functional and the corresponding PBE Goedecker−Teter−Hutter pseudopotentials for core electrons.[76−78] A 400 Ry density CUTOFF criterion with the finest grid level was employed, together with multigrids number 5 (NGRID 5 and REL_CUTOFF 30) using the smoothing for the electron density (NN10_SMOOTH) and its derivative (NN10).[74] A correction for dispersion interactions has been added by using the DFT-D3-type pair potential.[79,80] 1.0×10^{-6} has been chosen as the target accuracy threshold for the self-consistent field (SCF) convergence evaluation criteria. The DIIS minimizer was used to reach a faster orbital transformation via direct inversion in the iterative subspace.[73] The maximum number of SCF iterations to be performed for one iteration was set to 100, while a maximum of 10 iterations were performed for outer SCF loops. Periodic boundary conditions were applied to avoid boundary effects. With the aid of Nosé−Hoover chain thermostats with a time constant of the thermostat chain of 50 fs, the canonical (NVT) ensemble was used. A equilibration/relaxation over 5 ps has been performed defining the keyword REGION MASSIVE, so that for every degree of freedom of each single atom, a thermostat is used individually to achieve a faster equilibration. After the equilibration/relaxation part, this keyword was excluded. The production run was performed at a given temperature of 380 K and cover 190 ps for system A and 96 ps for system B. The time step was chosen to be 0.5 fs. During the production run, the Mulliken population analysis and the Blöchl method were applied every 200 steps to assign the partial charges on atoms.[81,82]

Analysis. Our open source program trajectory analyzer and visualizer (TRAVIS) was used to process the output trajectories of all of the simulations.[83] This tool offers different kinds of functions allowing the analysis of the interaction among the components of the systems. Intra- and intermolecular interactions can be taken into account. In this work, radial distribution functions (RDFs), number integrals (NIs), combined distribution functions (CDFs, as a combination of for example RDFs and angular distribution functions (ADFs)), Voronoi analysis, and calculated power spectra will have a main role to describe the interactions in play. The NI is obtained as integral of $g(r)$

$$N_c = 4\pi\rho \int_0^{r_{min}} r^2 g(r)\, dr \quad (1)$$

with N_c being the number of particles within the first solvation shell (from 0 to r_{min}, the first minimum of $g(r)$) and ρ the density. It allows us to determine the number of neighbors around a central atom, fragment, or virtual site (e.g., center of mass/ring/geometry). The integral to the first minimum of $g(r)$ gives the coordination number of the first shell neighbors, the

DOI: 10.1021/acsomega.8b00995
ACS Omega 2018, 3, 8567−8582

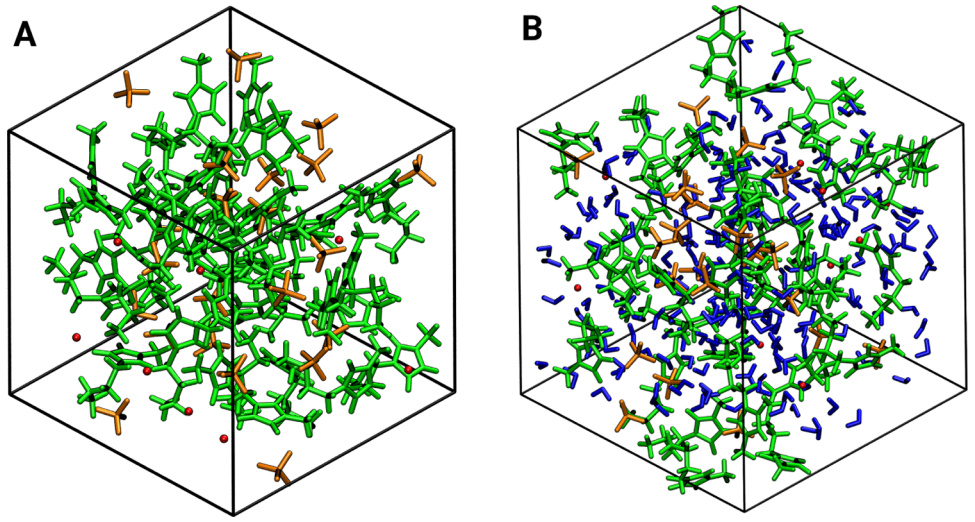

Figure 1. Simulation box for system A (left) and system B (right). Representation in licorice, color code: $[C_4C_1Im]^+$, green; $[BF_4]^-$, orange; $[Cl]^-$, red; and water, blue.

second minimum, the number of second shell neighbors, and so on. TRAVIS allows the user to choose a specific site of a structure (atom, center of the mass, or center of a ring (CoR)) to generate the distribution functions, enabling the user to discern between different interactions of the same pair of molecules. This feature is used to distinguish the three different hydrogen atoms on the imidazolium ring, the imidazolium center of the ring, and the different carbons of the imidazolium side chains. The nomenclature of the imidazolium cation atoms is shown in the labeling of Figure 2. All of the data obtained have been

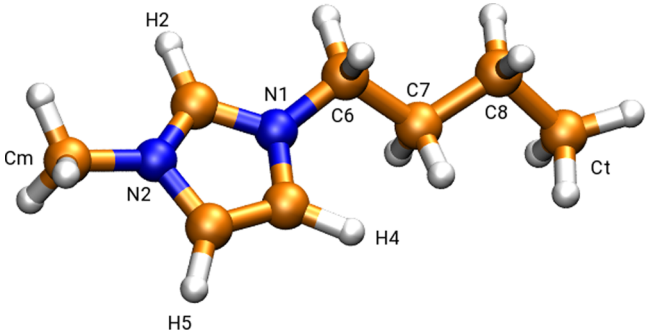

Figure 2. Labeling of different interaction sites on $[C_4C_1Im]^+$.

processed with either XMGRACE[84] or GNUPLOT[85] for the generation of the figures. To give a more specified insight into the structural behavior of our systems, domain analysis and radical Voronoi tessellation were performed.[86,87]

RESULTS

Ion Interplay. First insight into the behavior of the IL mixture under the influence of water can be gained by considering the interactions of ions in the two investigated systems, namely, the water-free system A and the water-containing system B. We will focus on interactions between counter ions because the like-ion-RDFs show the usual alternating pattern and thus were moved to the Supporting Information (SI).

We calculated the RDFs between the center of imidazolium ring (CoR) and the chloride atom (Cl) as well as the boron atom ($B(BF_4)$) of the tetrafluoroborate anion. Obviously, we expect the two anions to behave differently since the latter is weakly coordinating and the former is strongly coordinating. Furthermore, the $[Cl]^-$ is strongly hydrophilic, while the $[BF_4]^-$ anion can be characterized as less hydrophilic than $[Cl]^-$. Additionally, $[BF_4]^-$ can undergo hydrolysis.[88]

Figure 3 shows that in system A (dashed line) for CoR-$[Cl]^-$ (black) the first peak is twice as high as the one of the CoR-

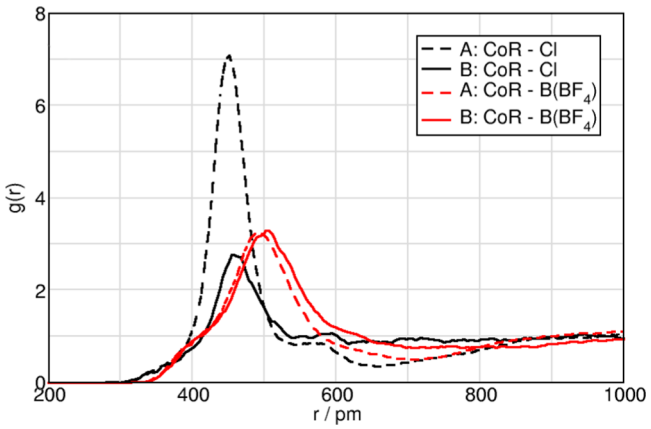

Figure 3. RDFs of the interaction between the center of imidazolium ring (CoR) and the anions in system A (dashed) and B (solid). Please note, for the $[BF_4]^-$ anion, the central boron atom is chosen to observe the overall polar (P) structure.

$[BF_4]^-$ (red) RDF, indicating a very directed interaction between $[Cl]^-$ and the cation. Furthermore, the cation−anion network is tighter when considering the $[Cl]^-$ anions as compared to the $[BF_4]^-$ anions, which is reflected in a much shorter location (40 pm) of the first peak; see Figure 3 and Table 2. In system B, the relations change such that the peak heights approach each other, with CoR-$[BF_4]^-$ being slightly higher, which is a typical effect of dilution. The chloride anion is still closer to the cation than the center of mass of the $[BF_4]^-$ anion.

Table 2 lists also the values of the NI and the $\overline{NI}$ at the first RDF minimum. Approximately, 5.6 and 5.3 cations surround the anions ($[Cl]^-$ and $[BF_4]^-$, respectively) in the water-free mixture. Addition of water leads to a reduction of the cation−anion coordination to 2.9 and 3.7; see Table 2 but also Figure 4.

DOI: 10.1021/acsomega.8b00995
ACS Omega 2018, 3, 8567−8582

Table 2. Distance of the First RDF Maximum and Minimum as Well as the Value of NIs at the First Minimum[a]

	X	$r(\text{X-Cl})_{max}$	$r(\text{X-Cl})_{min}$	NI	$\overline{\text{NI}}$
A	H2	239	455	0.5	1.7
A	H4	250	405	0.4	1.4
A	H5	251	405	0.4	1.4
A	CoR	452	700	1.8	5.6
B	H2	259	402	0.2	0.6
B	H4	270	402	0.1	0.4
B	H5	270	402	0.1	0.4
B	CoR	458	700	0.9	2.9
B	$H(H_2O)$	221			
	X	$r(\text{X-F})_{max}$	$r(\text{X-B})_{min}$	NI	$\overline{\text{NI}}$
A	H2	233	355	2.0	0.7
A	H4	235	355	1.5	0.6
A	H5	236	355	1.6	0.6
A	CoR	492*	700	3.6	5.3
B	H2	232	330	0.9	0.3
B	H4	236	330	0.8	0.3
B	H5	241	330	0.8	0.3
B	CoR	502*	700	2.5	3.7
B	$H(H_2O)$	209			

[a]$\overline{\text{NI}}$ gives the value for the atom combination the other way around; * indicates that X-B is used instead of X-F.

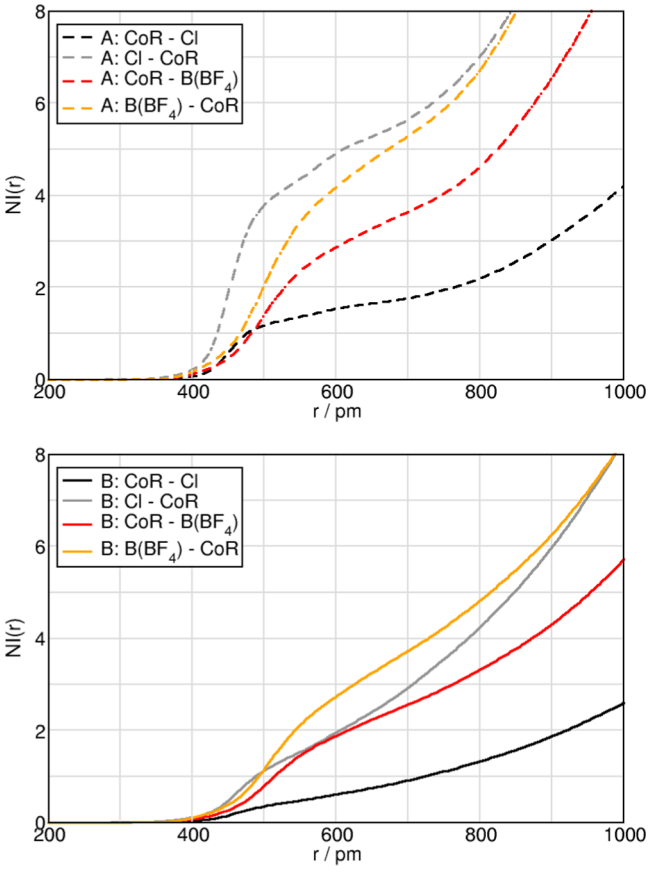

Figure 4. NIs (upper panel: system A and lower panel: system B) of the interaction between the center of imidazolium ring (CoR) and the anions. In the NI, the first atom (site) is surrounded by the amount of second atom (site), i.e., CoR-Cl indicates that the cation is surrounded by that many chlorides at a certain distance.

In the water-free system A, the cation is surrounded by twice as many $[BF_4]^-$ anions (3.6) as $[Cl]^-$ anions (1.8), which is exactly what one would expect with respect to the composition of the mixture. However, this is not the case in the moist mixture, where the cation is surrounded by 2.7 times more $[BF_4]^-$ than $[Cl]^-$ (2.5 vs 0.9). Interestingly, $[Cl]^-$ is surrounded by slightly more cations than $[BF_4]^-$ in system A; see the gray dashed curve compared to the orange dashed curve (Figure 4, upper panel). The opposite is the case in the moist mixture of system B with a reduced coordination number of approximately 2.9 and 3.7 for the cations surrounding the anions (Figure 4, lower panel).

Overall, it is apparent that the coordination number between the cation and the anion is reduced by water through interference of the cation−anion network. Note that, with respect to the four different water regimes in ionic liquids identified by Canongia Lopes,[48] the composition of this study lies in the bicontinuous system. The present x_{H_2O} is 0.87 calculated as in ref 48 from $n_{H_2O}/(n_{H_2O} + n_{IP})$ with n_{IP} being the number of ion pairs. The authors emphasize that $x_{H_2O} = 0.8$ can be considered as a threshold since many processes happen around that value, e.g., the average number of neighbors rapidly falls from ∼4 to just 2, indicating significant structural modifications in the polar network.

To further understand the perturbation of the Coulombic network, we also plot the anion−anion interaction in Figure 5.

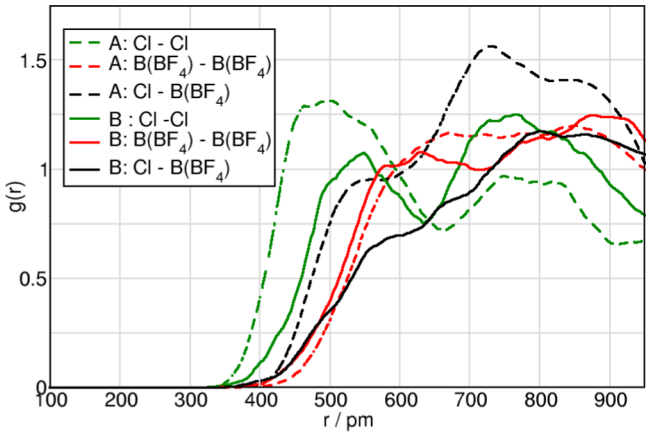

Figure 5. RDFs between the anion systems A (dashed line) and B (solid line).

We observe almost no changes for the $[BF_4]^-$ anion RDF with itself. Most significant is a slightly reduced interionic distance. In contrast to $[BF_4]^-$, the distance between the $[Cl]^-$ anions is increased significantly by water. This effect is also visible in the RDF characterizing the interplay of both anion types.

Hydrogen Bond Acceptor Interaction. The hydrogen bond acceptor capabilities of imidazolium-based ILs play a crucial role for physicochemical properties. The RDFs (Figure 6) show that water increases the distance between the hydrophilic $[Cl]^-$ anion and H2, H4, and H5 (also shown in Table 2 and the SI for H4 and H5), while the peak position of the hydrogen bond donor atom of the hydrophobic anion (F) is barely affected. The large peak height in system A indicates that the contact in the ionic liquid without water is very strong and thus directional (Figure 6), which is not the case for $[BF_4]^-$. This indicates that the $[Cl]^-$ anions transfer from being situated in the ionic liquid, in hydrogen bonds (HBs) with the cations, to the water continuum, while the $[BF_4]^-$ anion−cation interaction

DOI: 10.1021/acsomega.8b00995
ACS Omega 2018, 3, 8567−8582

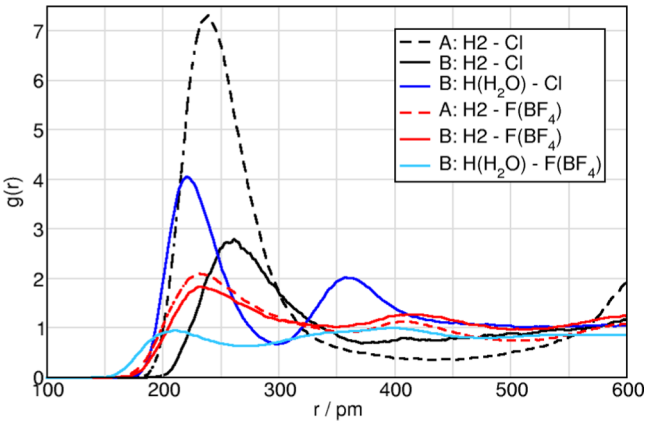

Figure 6. RDFs between the H2 hydrogen atoms and the contact atoms of the anions in systems A (dashed line) and B (solid line). The RDF for $H(H_2O)$ is also shown in blue.

is almost unperturbed, and in the water mixture, this interplay majorly contributes to the ionic liquid network.

Interestingly, the shortest HB acceptor distance can be observed for the proton of the "uncharged" water molecule with the anions and not between the counter ions. Since the HB distance is often linked to the hydrogen bond strength,[89] this indicates that the strongest hydrogen bond donor capabilities are displayed by water, which strongly reflect in the charge spreading; see section Spectroscopy for the detailed discussion. Please note that the distance between $H(H_2O)$ and F is shortest. However, $[Cl]^-$ possesses a larger van der Waals radius and, thus, a comparison of the HB distance between $[Cl]^-$ and F cannot be related to the HB length or directionality. This is supported by the first maximum of the F-$H(H_2O)$-RDF, which is below the statistical average and, thus, indicates overall poor HB interactions between water and the weakly coordinating anion.

According to the NIs (Table 2 and Figure 7), the H2 ring hydrogen atoms are surrounded in the first solvent shell by approximately 0.5 chloride anions and 2.0 fluor atoms of the $[BF_4]^-$ anions. This is reduced in water to values of 0.2 for the chloride anions and 0.9 for the fluor atoms of the $[BF_4]^-$ anions. Therefore, the strongest HB interactions between counter ions are reduced by 60% for the strong coordinating anion, while it is only reduced by 45% for the weak coordinating one.

It is known[89] that a strong hydrogen bond as in the water dimer can be more or less directional, i.e., the donor-H··· acceptor angles assume values of approximately 180°. The directionality of the hydrogen bond can be investigated by considering both acceptor atom−proton distance and the donor atom−proton−acceptor atom angle in combined distribution functions (CDFs). Figure 8 plots for the *x* axis the acceptor−proton distance and for the *y* axis the hydrogen bond angle. In system A, there are much more distinct areas for the H2···$[Cl]^-$ hydrogen bond than for the H2···$F(BF_4)$ hydrogen bond, indicated by the red area close to 180° for the $[Cl]^-$-CDF. In the presence of water, the situation changes such that the areas in the $[Cl]^-$-CDF are more smeared out and resemble much more the $[BF_4]^-$ map, showing that the linear hydrogen bond becomes less likely. Also, the on-top position (green area close to 0° and 600 pm) also losses probability, while the in-between regions are now more populated than in system A.

Solvation Structure of Water. So far we highlighted the influence of water on the interplay of ions and hydrogen bonds.

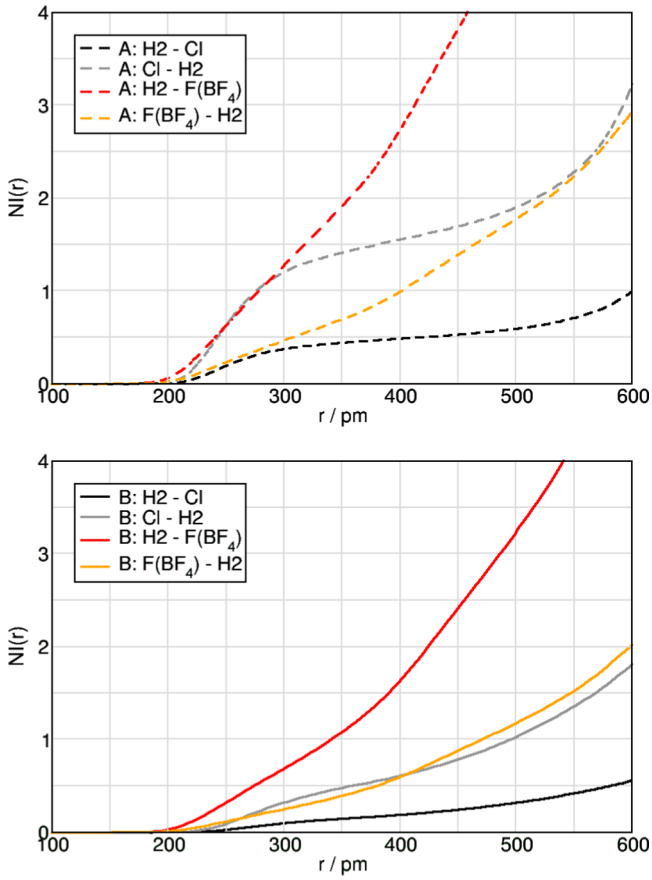

Figure 7. NI of system A (upper panel) and system B (lower panel) between the H2 hydrogen atoms and the contact atoms of the anions in systems A (dashed line) and B (solid line). Coordination has to be read like in Figure 4.

This section will focus on the solvation structure of water, which is depicted in Figure 9 and Table 3.

Water is closest to other water molecules (blue curve in Figure 9a) and assumes the usual hydrogen bonds, i.e., H···O of 186 pm and O···O distance of 286 pm; see Table 3. For the ions, the following order can be observed: the $[Cl]^-$ anion approaches water more and causes a much higher peak than the $[BF_4]^-$ anion, although it has to be kept in mind that the contact fluor atoms are able to assume shorter distances with the hydrogen atoms of water than the chlorine atoms; see Table 2. Below 400 pm, water sees more $[Cl]^-$ anions than cations or the other $[BF_4]^-$ anions, which can be attributed to the size of the ions; see the dark green curve in Figure 9, lower panel. That the strong coordinating $[Cl]^-$ anions are heavily solvated by water is apparent from the light green curve in Figure 9, bottom. Furthermore, the cation and the $[BF_4]^-$ anion are exposed to the water and share similar solvent shells of approximately six water molecules. Within the ionic liquid mixture, water shows a coordination number with respect to itself of 4.6; see Table 3. Therefore, water interacts strongly with all components as highlighted by the large NI.

Side Chain Behavior. To obtain a comprehensive picture, we also consider the behavior of the cation side chains. Long side chains in ionic liquids are known to induce microheterogeneity,[30,90] i.e., the nanosegregation between polar and nonpolar (NP) parts of the ionic liquids. Although these effects are usually only observed for side chains larger than a butyl side chain, first

DOI: 10.1021/acsomega.8b00995
ACS Omega 2018, 3, 8567−8582

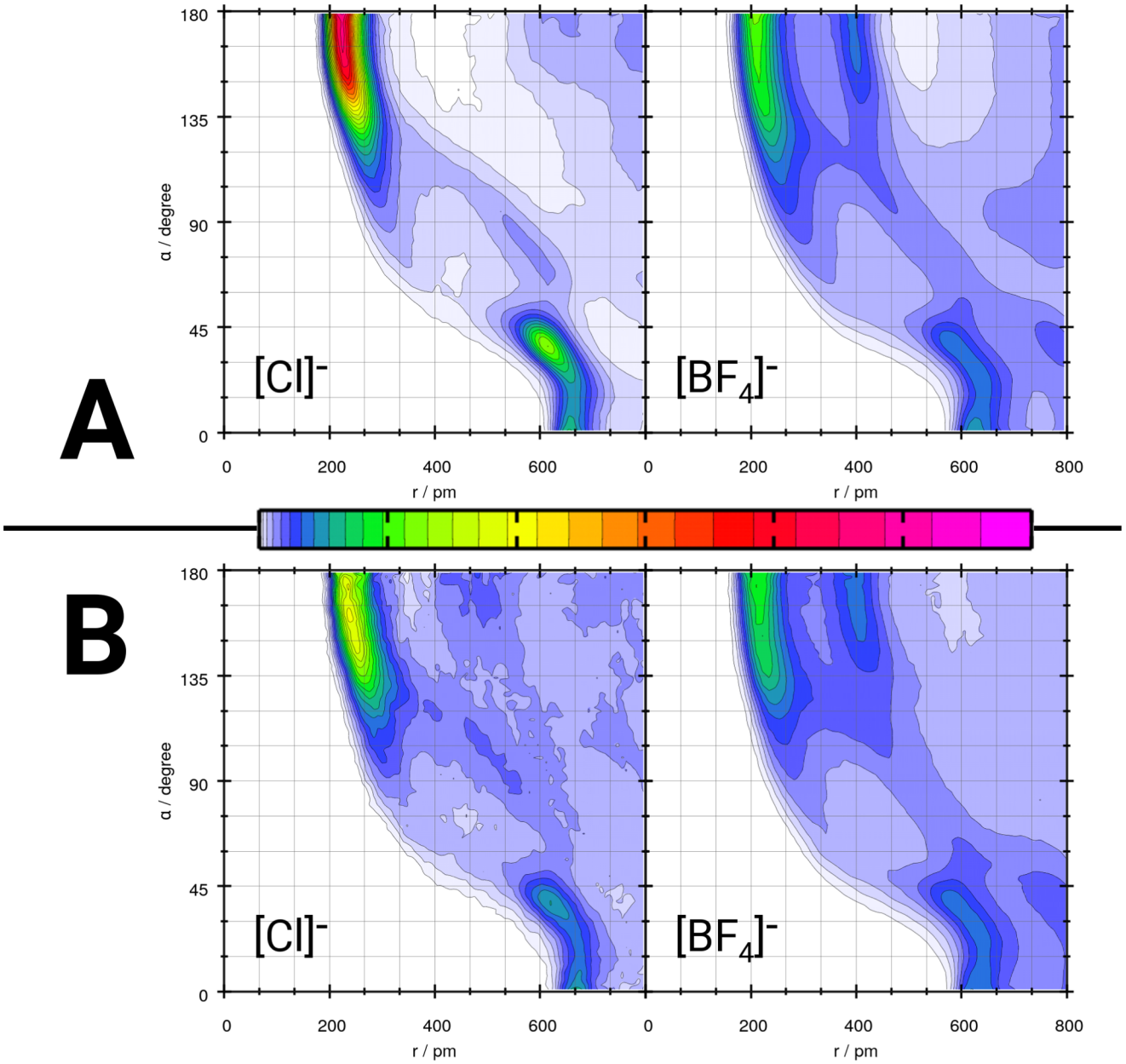

Figure 8. CDFs of the RDFs (*x* axis) and ADFs (*y* axis) for the hydrogen bond C2−H2···Cl (left) and C2−H2···F (right) in systems A (water-free, above) and B (water-containing, below). The RDF is calculated between H2 and the atom of the anion, while the angle is taken among C2, H2, and the atom of the anion.

indications for the side chain aggregation can also be observed with a butyl side chain.

In Figure 10 (upper panel), the RDFs for system A show stronger interaction for the terminal carbon atom of the butyl chain with their own species (dark green curve) than for the carbon atoms of the methyl groups with themselves (black curve) or the mixed interaction (red function). This is also reflected in the NIs (Figure 10, lower panel) which show that the terminal carbon atoms of the butyl group share more terminal carbon atom neighbors than the mixed interplay followed by the methyl group interaction with itself. Thus, in system A, the interaction between the butyl chains is the most favored. The situation changes slightly in the water-containing system, which shows that even the nonpolar parts of the ionic liquids are affected by the water addition, of course not to such a degree as the polar part of the ionic liquid. Interestingly, the interplay of the butyl chains with itself (Ct−Ct) is slightly reduced, which is visible in the RDF (Figure 10, upper panel), and the coordination numbers are sizably decreased, as indicated by the NIs (see Figure 10, lower panel), which is counterintuitive as one would assume that water makes the hydrophobic parts stick more together. The interaction between butyl chains and methyl groups become slightly more pronounced in the moist system than in system A. The methyl interaction with its own kind is strongly reduced so that the peak even assumes values smaller than 1.

Due to the small size of the anions, $\pi-\pi$ stacking seems possible. This enables the interaction of the methyl groups. The addition of water to the system leads to a weaker aggregation between cations and anions; consequently, the interaction between the cations is hindered. Figure 11 shows the CDF of the CoR−CoR distance and the angle between the two normal

DOI: 10.1021/acsomega.8b00995
ACS Omega 2018, 3, 8567−8582

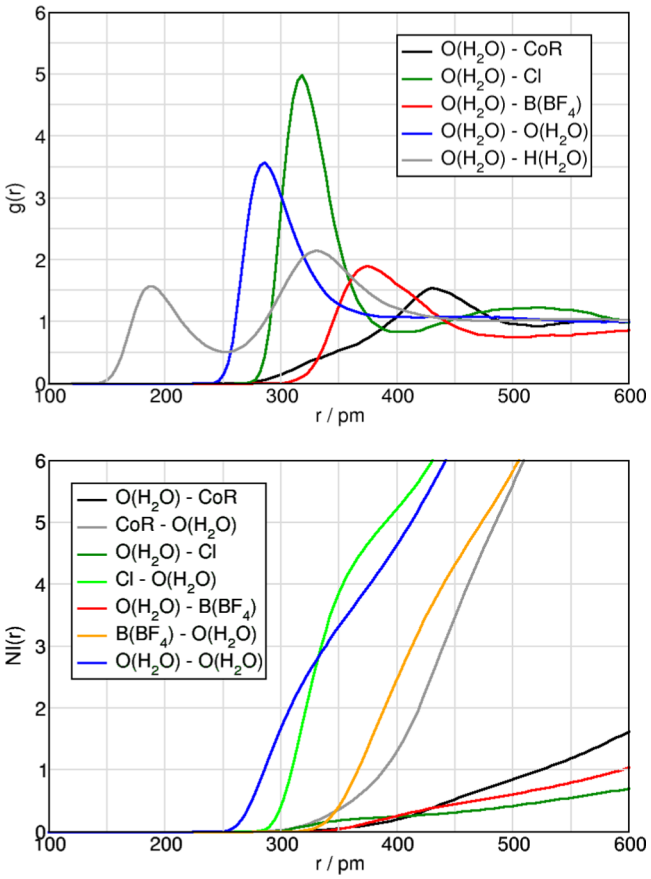

Figure 9. RDFs (upper panel) and NIs (lower panel) between the water oxygen and the center of ring, the chloride atom of the $[Cl]^-$ anion, and the boron atom of the $[BF_4]^-$ anion.

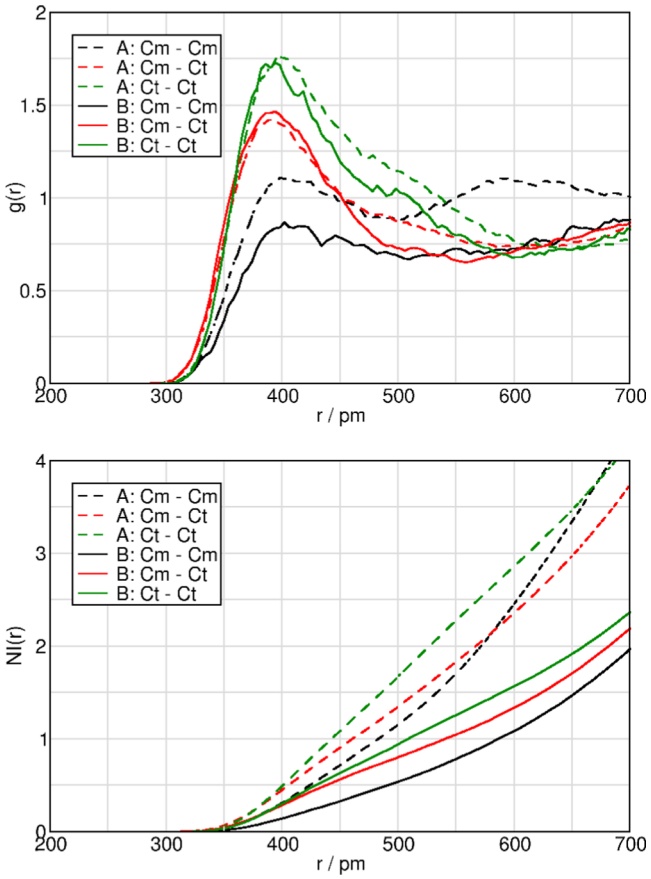

Figure 10. RDFs (upper panel) and NIs (lower panel) between different carbon atoms. Cm: methyl group; Ct: terminal carbon of the butyl chain in systems A (water-free) and B (water-containing). Please note that $\overline{NI}$ of Ct−Cm meets exactly Cm−Ct and therefore is not shown.

Table 3. Location of First Maximum (r_{max}), Minimum (r_{min}), and Number Integrals (NI/$\overline{NI}$) at the First Minimum[a]

	r_{max}	r_{min}	NI	$\overline{NI}$
CoR	430	522	6.5	1.0
Cl	318	398	5.2	0.2
$B(BF_4)$	374	510	6.2	0.6
$O(H_2O)$	286	400	4.6	
$H(H_2O)$	186	254		

[a]The first compound "sees" the amount of the water oxygen (NI) and vice versa ($\overline{NI}$).

vectors of neighbored imidazolium planes (as described in detail in the caption of the figure). A unique cation arrangement is highlighted by the red area for system A in this figure. The short CoR−CoR distance between 400 and 500 pm in combination with the parallel orientation of the N1−N2 vectors indicates $\pi-\pi$ stacking of the cations, already observed by means of NMR spectroscopy and theoretical approaches.[91,92] Furthermore, each nonpolar side chain prefers the contact to itself in this arrangement. There are a few high probable entries at 180°, which become more pronounced in the water-containing system B. Moreover, large changes can be observed for the parallel orientation in system B, i.e.; see lack of red area around 0−30° and 400−500 pm in Figure 11.

To further understand the water effect on the side chain of the cation in the ionic liquid mixture, we plot the intramolecular distance distribution of N1−Ct. This analysis reveals which conformation the side chain assumes; see Figure 12.[93] The conformation is determined by the arrangement of two units, namely, the N1−C6−C7−C8 unit and the C6−C7−C8−Ct unit. Both segments can hold a trans (t) or gauche (g) alignment, resulting in four different conformations tt, tg, gt, and gg. These conformations can be distinguished directly by the intramolecular N1−Ct distance. The little shoulder at 325 pm can be assigned as a conformation where the terminal carbon atom group sits on top of the imidazolium ring. Previously, we observed that this distribution is nearly anion-independent and that the gt and tg conformations are most probable.[93] This is in agreement with our system A simulation. Interestingly, we loss tt conformations and gain gg due to the addition of water. Thus, water crumbles the butyl side chains. This unexpected behavior might be a result of the preferred parallel orientation of the N1−N2 vectors in the pure IL system, which pushes the butyl chain into the linear arrangement. In a gg arrangement, the alkyl chain above the imidazolium plane is in competition with a $\pi-\pi$ stacking structure. However, the major contribution to the structure of the pure ionic liquid system is the Coulombic interactions, while the van der Waals interactions of the nonpolar chains play a minor role. Therefore, the addition of water allows a higher mobility of the nonpolar butyl chain facilitated by a more flexible cation arrangement to each other. This must have severe consequences when considering such mixtures with water in extraction processes in which the nonpolar nanophase plays a role.

DOI: 10.1021/acsomega.8b00995
ACS Omega 2018, 3, 8567−8582

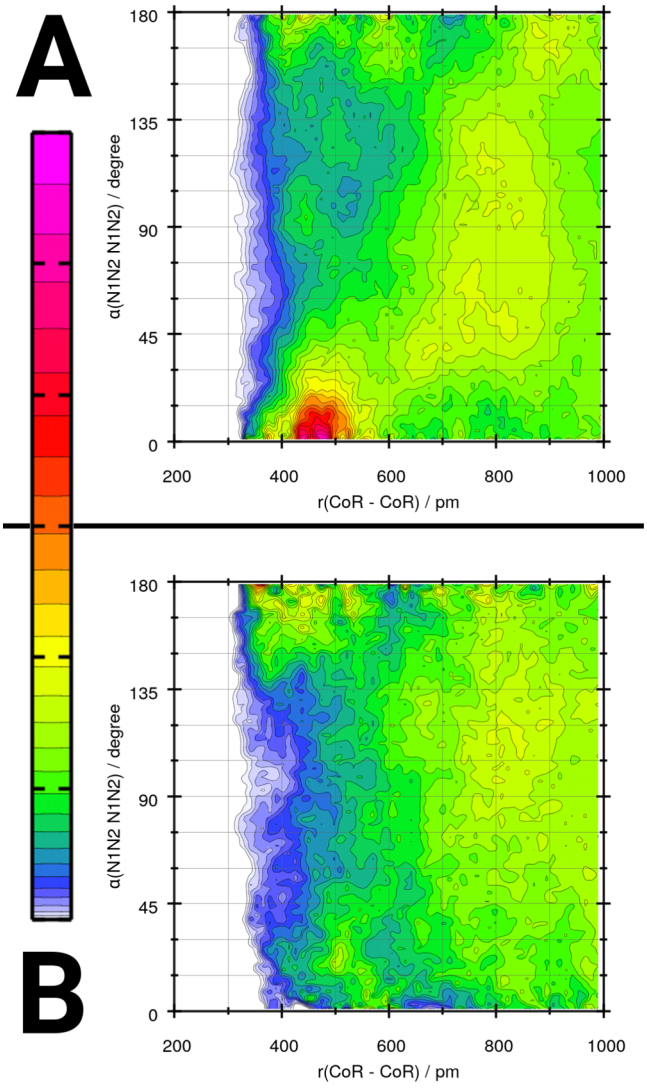

Figure 11. CDFs of the RDFs (x axis) and ADFs (y axis) for the cation orientation with respect to another cation in systems A (upper panel) and B (lower panel). The RDF is calculated between CoR and CoR, while the angle is taken between N1 and N2 vectors (see labels in Figure 2).

Voronoi Analysis. With the aid of our Voronoi analysis,[86,87] we can dissect the molecules of a condensed system into subsets and check connectivities and neighborhood relations within the system. Small numbers indicate a very connected microphase with number 1 pointing to completely connected subgroups. Larger numbers indicate that this kind of subset is dispersed in the liquid rather than connected. Turning next to this Voronoi analysis, we show in Table 4 the number of domains. The liquids are divided into polar (P: all polar parts) and nonpolar (NP: the propyl rest of the butyl chain) subsets as well as into polar ionic (P_{ion}), nonpolar (NP), and water (H_2O) subsets. Furthermore, we include a subset in which we add the $[Cl]^-$ anion to the water subset (H_2O + Cl) and consider both separately from polar ionic (P_{ion}) and the nonpolar (NP) group to find out whether the $[Cl]^-$ anions migrate into the water microphase.

As previously observed for several pure imidazolium-based ionic liquids,[30,86,87,90] dissecting the liquid into polar and nonpolar subsets leads to one connected polar domain in system A as well as in system B; see Table 4. While the nonpolar domain also forms one connected domain (this is next to the chain length dependent on the spacer between side chain and ring) in system A, the complete connection between nonpolar subsets is broken in the moist system, clearly indicating the intrusion or mixing of water with the ionic structure. More insight is provided by the dissection into ionic polar, nonpolar, and water subsets. This reveals a polar ionic microphase that is perturbed by water. Interestingly, the "one domain" behavior of the ionic part is recovered if $[Cl]^-$ is considered as a part of the water domain. This indicates that the Cl anions are taken up in a water environment.

Complementary insight is obtained from the surface coverage in Table 5. In many cases, there is a relatively high surface coverage by the side chain, which results from the side chain being chemically bonded to the polar part of the cation and the cation being the most abundant ionic species. Accounting for

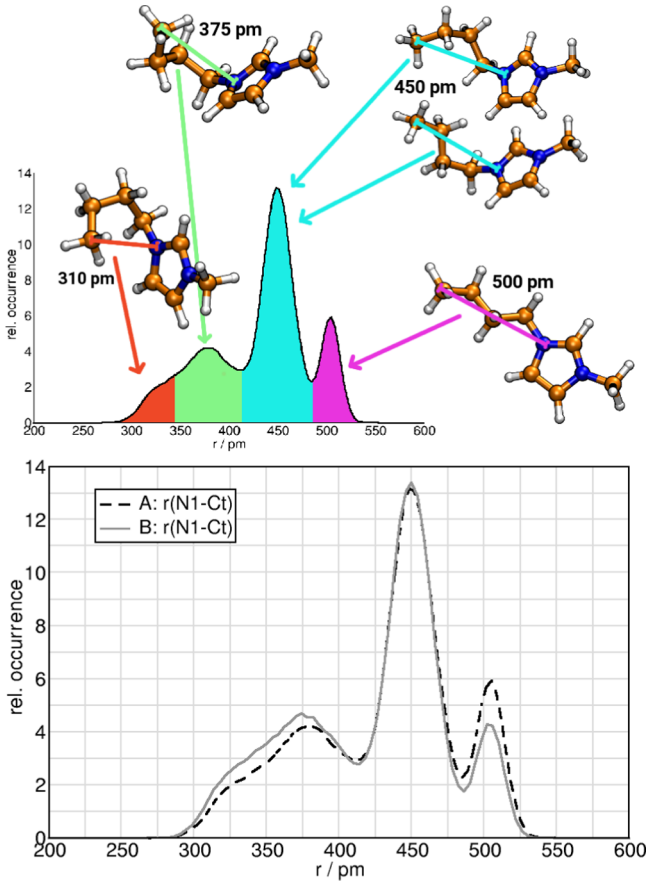

Figure 12. Side chain conformations of the cation. gg = gauche−gauche (orange), gt = gauche−trans (green), tg = trans−gauche (blue), and tt = trans−trans (purple) conformation. Assignment of histogram peaks and histogram of intramolecular N1−Ct distance of the cation. Solid lines: system B; dashed line: system A.

Table 4. Domain Voronoi Analysis for Systems A and B, First Column[a]

	P	NP	P_{ion}	NP	H_2O	P_{ion}-Cl	NP	H_2O + Cl
A	1.0	1.0	1.0	1.0		1.0	1.0	8.7
B	1.0	5.3	1.2	5.3	1.2	1.0	5.3	1.2

[a]Next block: dissection into polar (P: ring, methyl group, anion, water) and nonpolar (NP: butyl chain) subsets. Middle block: the dissection into polar ionic (P_{ion}: ring, methyl group, anions), nonpolar (NP: butyl chain), and water (H_2O). Last block: $[Cl]^-$ is subtracted from the polar subset and included in the water subset.

DOI: 10.1021/acsomega.8b00995
ACS Omega 2018, 3, 8567−8582

Table 5. Surface Coverage from Voronoi Analysis for Systems A and B[a]

	ring*	C_3H_7*	BF_4*	Cl*	H_2O*
			System A		
ring	27.8	49.8	65.3	81.0	
C_3H_7	35.7	28.9	31.3	16.8	
BF_4	28.4	19.0	3.0	1.8	
Cl	8.1	2.3	0.4	0.4	
			System B		
ring	12.3	36.5	39.0	25.5	20.0
C_3H_7	25.9	15.9	17.4	10.7	12.0
BF_4	16.8	10.5	2.2	0.6	8.4
Cl	2.5	1.5	0.1	0.0	2.9
H_2O	42.5	35.6	41.3	63.2	56.7

[a]The subsets are ring (ring of the cation plus methyl group plus the CH_2 space of the butyl side chain), C_3H_7 (the propyl rest of butyl side chain), BF_4 (atoms of $[BF_4]^-$), Cl ($[Cl]^-$), and water. * Indicates referred coverage, columns = observed surface (values given are in percentages).

both anions together in system A, it is obvious that the anions mostly spread over the surface of the ring. The $[BF_4]^-$ anions cover more of the ring than the $[Cl]^-$ anions. This even exceeds the factor two of the anion ratio and is related most likely to the size. The side chain is mainly covered by the ring (covalent bond), which is followed by other side chains to 28.9%. There is some sizable amount of $[BF_4]^-$ anions (19%) in the proximity of the butyl chain, while the chloride anion is rather absent (2.3%), reflecting the stronger hydrophobic behavior of $[BF_4]^-$. The anions are largely covered by the polar part of the cation with a higher coverage of the $[Cl]^-$ anions (81%) than that of the $[BF_4]^-$ anion (65.3%). Side chain coverage does play a role with a higher priority for the $[BF_4]^-$ anion.

Addition of water changes the situation drastically. Water covers each subset by more than 35% and, thus, each part of the IL network is perturbed significantly. Due to the high proportion of water, the coverage of each IL subset by the IL is reduced noticeably. The side chain coverage by other side chain subsets is reduced as well. The $[BF_4]^-$ anion suffers a similar reduction of the ionic liquid subset coverage as the polar part of the cation (ring). Although the overall coverage of the $[BF_4]^-$ anion with the cation is reduced, in the moist system, it is now more covered by the cation (39.0%) than the chloride anion (25.5%). In fact, the most pronounced changes can be observed for the $[Cl]^-$ anions: the 81% surface coverage by the ring subset is reduced to 25.5%, while the coverage of the anions by water is 63.2%.

Dynamical Properties. While structural information is important with respect to arrangements in the liquids, dynamical properties help to estimate availability and mobility. Insight into the lifetime of certain aggregates can be obtained in terms of continuous autocorrelation functions.[94]

In Figure 13, we display the continuous autocorrelation functions.[94] Obviously, all investigated dynamical properties are significantly accelerated by water, which is visible by the faster decay of the autocorrelation functions. In the water-free IL mixture, the strongly coordinating Cl^- anion center of the ring aggregate decays more slowly than the weakly coordinating $[BF_4]^-$ anion aggregate, which also indicates that in the competition of the anions for the cation, the strongly coordinating anion succeeds. The situation changes when water is added. In the water-free system, the strongest hydrogen donor site constitutes the H2 position at the cation, see Figures 6 and 8, and in the water-containing system, this role is taken by the proton from H_2O. This is the reason why not only the aggregates decay faster in general but also the CoR-anion groups reverse their order. While the CoR-Cl clusters possess a longer lifetime than the CoR-BF_4-aggregates in the water-free system, this trend is reversed by the addition of water. Keeping in mind that water is a fluctuating network of hydrogen bonds, it is not surprising that the aggregates formed with water show this order of mobility. It is well-known that an intermittent function[95] or even one based on the reactive flux theory[96,97] would describe the process with the fluctuating water better. Unfortunately, the accessible simulation runtime is too short for this kind of analysis.[94]

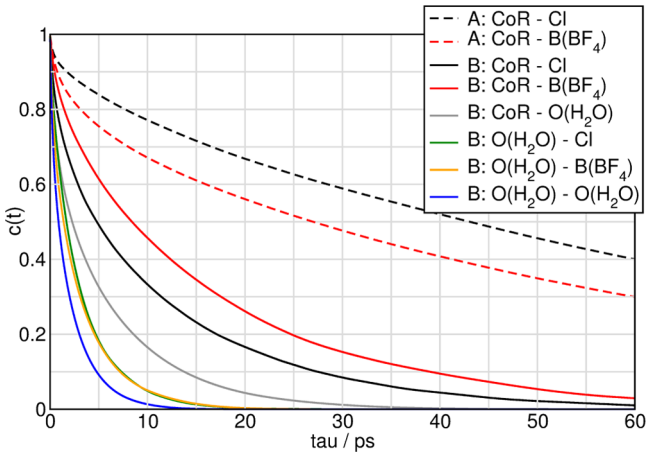

Figure 13. Continuous autocorrelation of the aggregates based on a distance criterion of 700 pm for CoR-anions. The other aggregate was determined at approximately their first minimum in the RDF, which is 400 pm for O−O and O−Cl and 500 pm for O−B(BF_4).

To analyze the effect of water addition on the transport properties of ILs, we determined the mean square displacement (msd) of the CoR of the cations and the central atoms of the anions. Figure 14 shows that the msd for both anions and cations is similar, within the uncertainty of the calculations as previously observed in AIMD. Due to the fact that the sampling for this property is too short and the system size too small, we obviously do not calculate diffusion constants.[98,99] Nevertheless, trends with respect to adding water on the msd curves can be considered. While the CoR's of the cation and the chloride anion

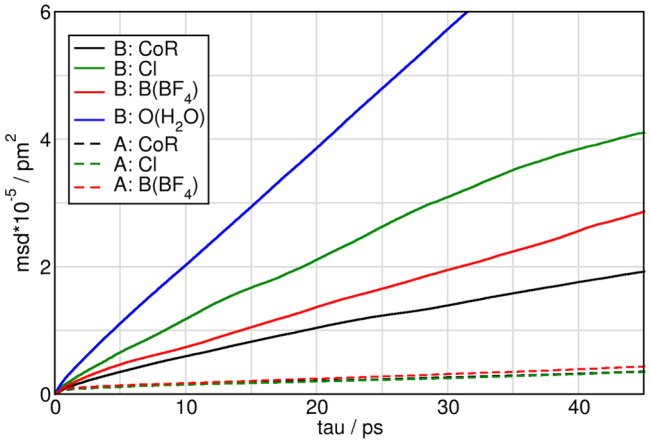

Figure 14. Mean square displacement of the ions and water in system A (dashed lines) and in system B (solid line).

DOI: 10.1021/acsomega.8b00995
ACS Omega 2018, 3, 8567−8582

diffuse similarly in system A, the $[BF_4]^-$ anions seem to be more mobile. This order changes in the moist system B in which the chloride anions seem to be much more mobile than the $[BF_4]^-$ anions and the cation. While the order of the mobility could still be a result of insufficient sampling, the acceleration of the ion dynamics by water is too strong and clearly an effect of water, confirmed by experimental observations. Of course, water is much more mobile than any other compound in the system. These conclusions are also in line with a previous work by Maginn and co-workers,[100] in which they study the influence of water on different neat ionic liquids, showing that water has different effects depending on the nature of the anions.

Charge Analysis. In the following section, we carry out a charge analysis. The obtained absolute values depend on many criteria, some of them already arise from the setup of our simulations, but most important is of course the method for the charge calculation itself. Therefore, our main objective is not to get absolute numbers for our partial charges, but the distribution of these. Through this approach, we are able to observe the influence of the polarization effects on the electron density of our system and as a result on our partial charges. As mentioned before, two different methods have been used for the assignment of the charges (the Blöchl and Mulliken methods). Hereby, we report the charges derived using the Blöchl method as it can deal with dense systems and periodic boundary conditions.[101] However, it is important to note that Mulliken and Blöchl are in agreement with each other. Figure 15 shows the charge

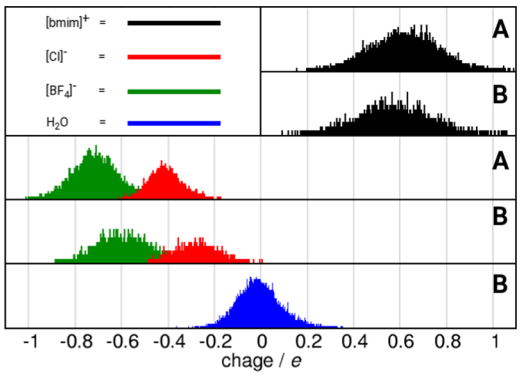

Figure 15. Comparison of the total charge distribution of the cations, anions, and water molecules in systems A and B.

distributions for the cations, anions, and water molecules, in systems A and B. In system A, the total average charge on the cation is 0.62*e*, on $[Cl]^-$ is −0.41*e*, and on $[BF_4]^-$ is −0.71*e*. In system B, the total average charge on the cation is 0.57*e*, on $[Cl]^-$ is −0.27*e*, on $[BF_4]^-$ is −0.59*e*, and on H_2O is −0.01*e*. The perk of this visualization is that it allows us to appreciate that charges are not fixed but they vary along the simulation and that they fluctuate, following a distribution, which recall the Gaussian one. It is noteworthy that at half-height of the Gaussian, the values can still vary in a range of 0.4*e* in the case of the cations and 0.2*e* in the case of the anions and water molecules. Those ranges of "freedom" are reduced to about half when the Mulliken method is taken into account (SI). Concerning the position of the maximum of those distributions, we see that considering system B instead of system A reduces the absolute value of the charge of the cations and the anions; see Figure 15. In other words, cations and anions are losing their charge (which is especially evident in the case of the anions), which is originated by the charge transfer to water molecules. The charge transfer is also confirmed by the position and shape of the charge distribution of the water molecules. In fact, the water charge distribution exhibits a shoulder on the negative side, which implies that part of the charge of the anions has been shifted on the water molecules. Another fascinating fact is given by the relative position of the charge distributions of the anions. In both analysis (Blöchl and Mulliken), $[Cl]^-$ is more positive than $[BF_4]^-$, which is in line with the already described stronger interaction of this anion with the cations and which consequently leads to a more pronounced charge transfer. Noteworthy is that compared to the cation charge distributions, the anion charge distributions are more influenced by the presence of water molecules.

Figure 17 depicts the charge distribution of different groups, belonging to the side chains of the cations. Although a significant difference between systems A and B is not observable, the wide distribution of the overall charge of these groups is interesting. In fact, when we compare the overall charges of the same groups in classical the molecular dynamics force field, we find some differences (see Figure 16). Such a comparison is made to

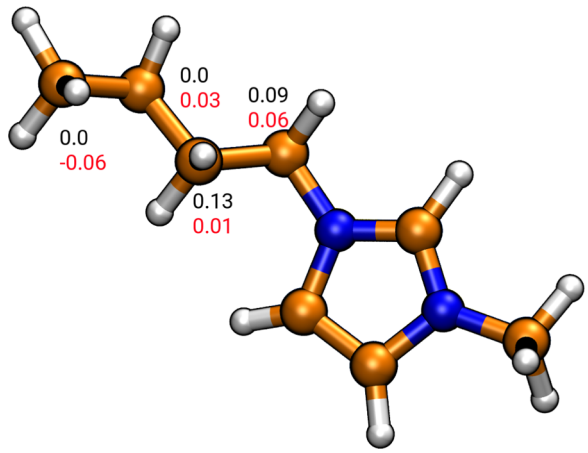

Figure 16. Charges on the groups (methylene and methyl) of the side chain of the cation. In black are shown the charges from Canongia Lopes and Pádua force field, and in red are shown the average charges in system A calculated by means of the Blöchl method.

underline how much those values change once polarization and charge transfer have occurred and to guide future force field developments. In Canongia Lopes and Pádua force fields, which are among the most used, the methyl group carries an overall charge of 0.22*e* and the first methylene of the butyl chain carries a charge of 0.09*e*. In our evaluation, those two charges are nearly identical (see Figure 17, black and purple distributions, charge = 0.06*e*). When we consider the second methylene group of the butyl chain, the overall charge of the force field is 0.13*e*, slightly higher than that of the first methylene group (0.09*e*). Compared with the Canongia Lopes and Pádua force field, our results are clearly different. In fact, for the second methylene group, the average total charge is 0.01*e*, which is lower than the charge on the first methylene group (0.06*e*). The third methylene group and the terminal methyl group of the butyl chain in the force field are described by means of the opls-aa charges, and the overall charge for both of them is 0. The calculated charges for these groups are, respectively, 0.03*e* and −0.06*e*. Nevertheless, those qualitative differences are not surprising when one takes into account that to obtain the charges for the force field, static quantum chemical calculations have been used. Those

DOI: 10.1021/acsomega.8b00995
ACS Omega 2018, 3, 8567−8582

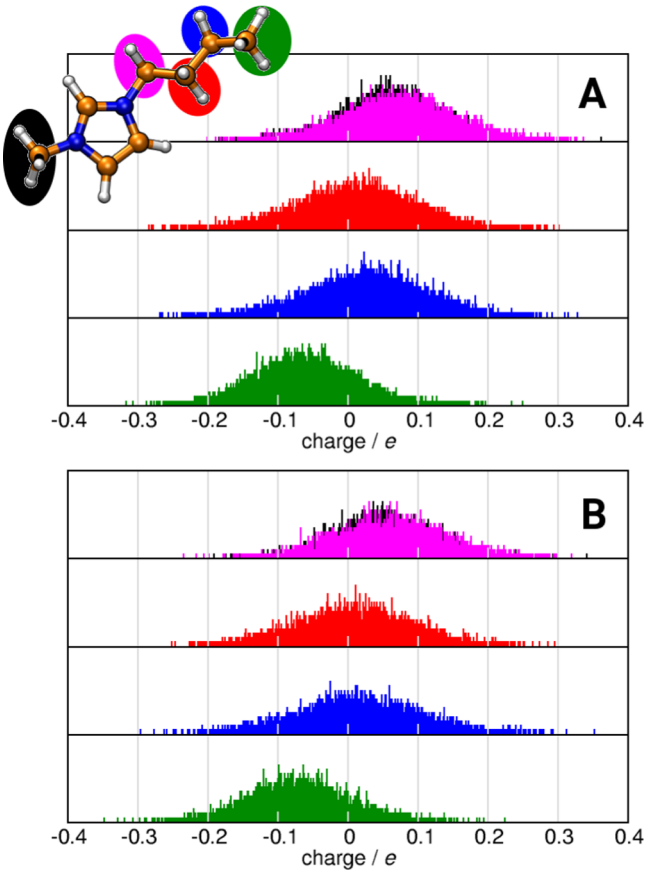

Figure 17. Comparison of the partial charge distribution of different groups belonging to the side chains of the cations in systems A and B.

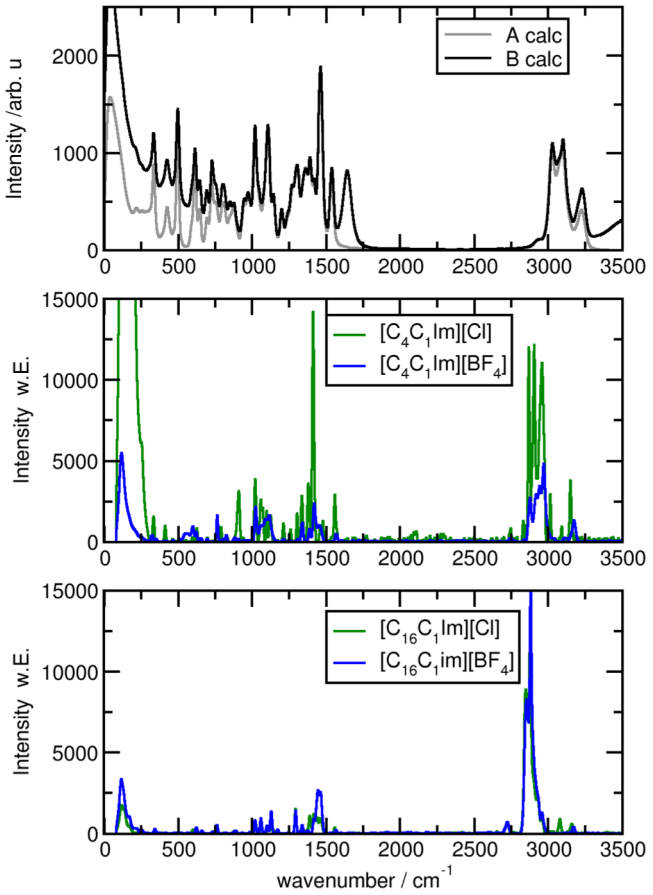

Figure 18. Upper panel: complete power spectrum calculated for system A (gray) and system B (black). Middle panel: experimental Raman spectrum of pure $[C_4C_1Im][Cl]$ and $[C_4C_1Im][BF_4]$. Lower panel: experimental Raman spectrum of pure $[C_{16}C_1Im][Cl]$ and $[C_{16}C_1Im][BF_4]$.

calculations are typically performed on single optimized molecules (or ions in this case) in vacuum, and they do not take into account the solvation of the molecules.

Spectroscopy. It is possible to obtain the vibrational density of states (VDOSs) from an MD trajectory as the power spectrum (Fourier transform of the time autocorrelation function of the atomic velocities, VACF). Figure 18 compares the VDOSs obtained from the VACF of the two systems A and B (upper panel) with experimentally obtained Raman spectra of pure $[C_4C_1Im][Cl]$ and $[C_4C_1Im][BF_4]$ (middle panel).

The observed results with (black) and without (gray) water content are quite close, and the general shape of the spectrum is similar in both cases. Nevertheless, three features with respect to water should be specially mentioned: first, the spectrum obtained from the trajectory with water gains intensity in the low-wavenumber region due to the modes related to the movement of the heavy atoms; see also Figure 19 in which the spectra are decomposed with respect to the different compounds. Second, it has one additional peak at around 1640 cm^{-1}, which is due to the water bending motion. Third, there are some entries above 3300 cm^{-1}, which are related to the O−H stretch modes. However, there are also changes with respect to the ionic liquid ions. Up to 1200 cm^{-1}, the $[BF_4]^-$ anion shows entries; see Figure 19 (upper panel, orange spectrum). Upon water addition, there is a loss of intensity, and below 300 cm^{-1}, the modes are shifted to lower wavenumbers. In the low-wavenumber region, the cation features ring breathing. Between 500 and 1000 cm^{-1}, the modes originating from vibrations involving carbon atoms are visible. The peaks between 2800 and 3000 cm^{-1} stem from the butyl chain attached to the imidazolium ring,[98,102] which are attributed to the stretching and Fermi resonance modes of CH_2 and CH_3. Features between 3000 and 3200 cm^{-1} are attributed to the C−H vibration modes of the imidazolium ring.[98,102]

It is possible to compare the predictions of our calculations with the experimental Raman spectrum. The agreement is satisfactory: the global form of the experimental spectrum is well reproduced from the DFT calculations. The calculated spectrum shows a red shift of the modes in the high wavenumbers when compared with the experimental data.

CONCLUSIONS

By means of ab initio molecular dynamics simulations, in this article, we have studied the ionic liquid mixture composed of three components $[C_4C_1Im]^+$, $[BF_4]^-$, and $[Cl]^-$ without and with water to understand the effect of water on an ionic liquid mixture as it is applied in material synthesis.[9,10] This is the first AIMD study investigating the effect of water on an ionic liquid mixture.

For our particular composition (i.e., 0.87 mole fraction x_{H_2O}), we observe a strong perturbation of the ionic liquid network by water in which the cation−anion coordination numbers are strongly reduced. While the $[BF_4]^-$ anion interplay with itself remains almost the same when adding water, the other like-ion interactions ($[Cl]^-$ with itself and interacting with the $[BF_4]^-$ anion) change such that these become less probable. The strong

DOI: 10.1021/acsomega.8b00995
ACS Omega 2018, 3, 8567−8582

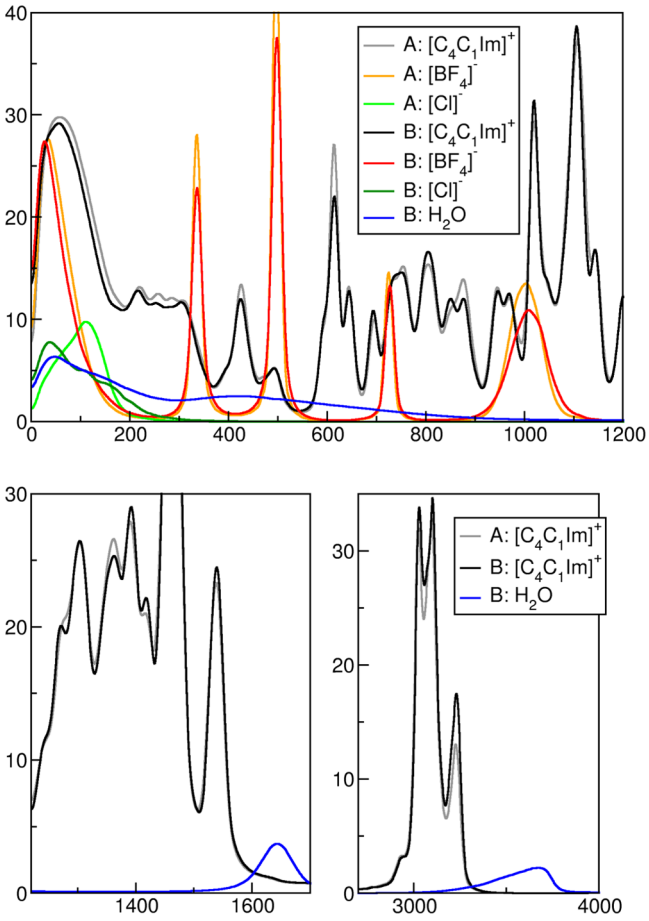

Figure 19. Power spectrum decomposed for the particular ions.

directional coordination between the ring hydrogen atoms and chloride is tremendously reduced, and chloride forms strong hydrogen bonds with water, while the weakly coordinating $[BF_4]^-$ anions though being in contact with water show almost no particular hydrogen bond contacts to water. The amount of water added even influences the side chain behavior, though to a lesser extent. The side chain crumbles more compared with the pure mixture, and the orientation of the cation with respect to other cations is now more random. An interesting insight is obtained from the Voronoi tessellation analysis of the domain count and the surface coverage. As usual, in ionic liquids, the polar network in the IL mixture without water is one connected domain and the nonpolar side chains also form one domain, which generally depends on the spacer and the chain length. Addition of water disperses the side chain aggregation, independently whether water is counted as extra subset or added to the polar part of the IL mixture. Dispersed nonpolar groups usually can be found when short side chains are chosen or when large anions form the ionic liquids. Additionally, the polar ionic groups are now slightly dispersed, which usually is never observed for a water-free ionic liquid. The distinction of a polar ionic and the water subset clearly shows that the $[Cl]^-$ anions are "pulled" into the water continuum. Similar conclusions can be drawn from the surface coverage. While in the pure mixture, the dominance of the cation coverage by the $[BF_4]^-$ anion is only a factor of 3.5, it changes when water is added to a factor of 6.7. In the pure mixture, the coverage of the strongly coordinating $[Cl]^-$ anion is to 81% by the polar part (ring) of the cation and it is only to 65.3% for the $[BF_4]^-$ anion. This coverage is reduced in total, and the priority is changed when water is added. Even more strikingly, the ring coverage of the water-containing system (25.5%) is much less than that of the water coverage (63.2%) of the $[Cl]^-$ anion.

Addition of water to ionic liquids might in principle lead to an increase in nanosegregation and domain formation for the nonpolar part of the ionic liquid. However, in this particular system, water strongly interacts with the $[Cl]^-$ anions and "pulls" them out of the polar ionic liquid network. The side chain is thus more exposed to an IL network with large anions and thus becomes more dispersed in the system. The charge analysis, which reflects the electronic structure of our systems, yields further insights into the dynamical situation of our investigated systems and the crucial role of polarization effects of those. Noteworthy is the charge transfer from the anions to the water molecules and the different arrangement and shape of the charge distribution of $[BF_4]^-$ and $[Cl]^-$ with respect to their coordination behavior. These observations have large impacts on the applications of ILs to all of the different fields: they show how different modifications of nanostructuring can be obtained by adding the right components to a mixture and how they can be dissolved. They also show that different components can be made available by transferring them from one microcontinuum to the other. These possibilities have to be thoroughly understood to make them optimal for material synthesis, in energy devices, or in separation processes. Furthermore, our study has impacts on systems with added salting-out or coordinating agents. As shown in this study, if one chooses an ionic liquid mixture in which components of the IL already play this role, the addition of such agents might be redundant because those can be contained in the solvent itself.

■ ASSOCIATED CONTENT

Supporting Information

The Supporting Information is available free of charge on the ACS Publications website at DOI: 10.1021/acsomega.8b00995.

Like-ion RDFs; acidic hydrogen atom competition; partial charge analysis, Mulliken (PDF)

■ AUTHOR INFORMATION

Corresponding Author

*E-mail: kirchner@thch.uni-bonn.de.

ORCID

Bernd M. Smarsly: 0000-0001-8452-2663

Barbara Kirchner: 0000-0001-8843-7132

Notes

The authors declare no competing financial interest.

■ ACKNOWLEDGMENTS

The authors acknowledge the priority program 1708 under the project KI 768/15-1 and SM 199/11-1. Furthermore B.K. and R.M. greatly thank the ETN Socrates (http://etn-socrates.eu/) because this project has received funding from the European Union's EU Framework Programme for Research and Innovation Horizon 2020 under Grant Agreement No 721385.

■ REFERENCES

(1) Armand, M.; Endres, F.; MacFarlane, D. R.; Ohno, H.; Scrosati, B. Ionic-liquid materials for the electrochemical challenges of the future. *Nat. Mater.* **2009**, *8*, 621−629.

(2) Navarra, M. A.; Fujimura, K.; Sgambetterra, M.; Tsurumaki, A.; Panero, S.; Nakamura, N.; Ohno, H.; Scrosati, B. New Ether-

DOI: 10.1021/acsomega.8b00995
ACS Omega 2018, 3, 8567−8582

functionalized Morpholinium- and Piperidinium-based Ionic Liquids as Electrolyte Components in Lithium and Lithium-Ion Batteries. *ChemSusChem* **2017**, *10*, 2496−2504.
(3) Díaz, M.; Ortiz, A.; Ortiz, I. Progress in the use of ionic liquids as electrolyte membranes in fuel cells. *J. Membr. Sci.* **2014**, *469*, 379−396.
(4) Salanne, M. Ionic Liquids for Supercapacitor Applications. *Top. Curr. Chem.* **2017**, *375*, 63.
(5) Lin, Z.; Goikolea, E.; Balducci, A.; Naoi, K.; Taberna, P.; Salanne, M.; Yushin, G.; Simon, P. Materials for supercapacitors: When Li-ion battery power is not enough. *Mater. Today* **2018**, *21*, 419−436.
(6) Lewandowski, A.; Galinski, M. Carbon-ionic liquid double-layer capacitors. *J. Phys. Chem. Solids* **2004**, *65*, 281−286.
(7) Abbott, A. P.; McKenzie, K. J. Application of ionic liquids to the electrodeposition of metals. *Phys. Chem. Chem. Phys.* **2006**, *8*, 4265−4279.
(8) Binnemans, K. Lanthanides and Actinides in Ionic Liquids. *Chem. Rev.* **2007**, *107*, 2592−2614.
(9) Voepel, P.; Seitz, C.; Waack, J. M.; Zahn, S.; Leichtweiss, T.; Zaichenko, A.; Mollenhauer, D.; Amenitsch, H.; Voggenreiter, M.; Polarz, S.; Smarsly, B. M. Peering into the Mechanism of Low-Temperature Synthesis of Bronze-type TiO_2 in Ionic Liquids. *Cryst. Growth Des.* **2017**, *17*, 5586−5601.
(10) Santner, S.; Yogendra, S.; Weigand, J. J.; Dehnen, S. Exploring the Chemical Reaction Space at the Formation of Chalcogenidometalate Superspheres in Ionic Liquids. *Chem. − Eur. J.* **2017**, *23*, 1999−2004.
(11) Groh, M. F.; Mueller, U.; Ahmed, E.; Rothenberger, A.; Ruck, M. Substitution of conventional high-temperature syntheses of inorganic compounds by near-room-temperature syntheses in ionic liquids. *Z. Naturforsch. B* **2013**, *68*, 1108−1122.
(12) Elfgen, R.; Hollóczki, O.; Ray, P.; Groh, M. F.; Ruck, M.; Kirchner, B. Theoretical Investigation of the Te_4Br_2 Molecule in Ionic Liquids. *Z. Anorg. Allg. Chem.* **2017**, *643*, 41−52.
(13) Hallett, J. P.; Welton, T. Room-Temperature Ionic Liquids: Solvents for Synthesis and Catalysis. 2. *Chem. Rev.* **2011**, *111*, 3508−3576.
(14) Holbrey, J. D.; Seddon, K. R. Ionic Liquids. *Clean Technol. Environ. Policy* **1999**, *1*, 223−236.
(15) Wessel, C.; Zhao, L.; Urban, S.; Ostermann, R.; Djerdj, I.; Smarsly, B. M.; Chen, L.; Hu, Y.-S.; Sallard, S. Ionic-Liquid Synthesis Route of TiO_2(B) Nanoparticles for Functionalized Materials. *Chem. − Eur. J.* **2011**, *17*, 775−779.
(16) Balducci, A.; Bardi, U.; Caporali, S.; Mastragostino, M.; Soavi, F. Ionic liquids for hybrid supercapacitors. *Electrochem. Commun.* **2004**, *6*, 566−570.
(17) Balducci, A.; Henderson, W. A.; Mastragostino, M.; Passerini, S.; Simon, P.; Soavi, F. Cycling stability of a hybrid activated carbon// poly(3-methylthiophene) supercapacitor with N-butyl-N-methylpyrrolidinium bis(trifluoromethanesulfonyl)imide ionic liquid as electrolyte. *Electrochim. Acta* **2005**, *50*, 2233−2237.
(18) Balducci, A.; Dugas, R.; Taberna, P.-L.; Simon, P.; Plee, D.; Mastragostino, M.; Passerini, S. High temperature carbon-carbon supercapacitor using ionic liquid as electrolyte. *J. Power Sources* **2007**, *165*, 922−927.
(19) Appetecchi, G. B.; Montanino, M.; Balducci, A.; Lux, S. F.; Winterb, M.; Passerini, S. Lithium insertion in graphite from ternary ionic liquid-lithium salt electrolytes: I. Electrochemical characterization of the electrolytes. *J. Power Sources* **2009**, *192*, 599−605.
(20) Pohlmann, S.; Lobato, B.; Centeno, T. A.; Balducci, A. The influence of pore size and surface area of activated carbons on the performance of ionic liquid based supercapacitors. *Phys. Chem. Chem. Phys.* **2013**, *15*, 17287−17294.
(21) Béguin, F.; Presser, V.; Balducci, A.; Frackowiak, E. Carbons and electrolytes for advanced supercapacitors. *Adv. Mater.* **2014**, *26*, 2219−2251.
(22) Tazi, S.; Salanne, M.; Simon, C.; Turq, P.; Pounds, M.; Madden, P. A. Potential-induced ordering transition of the adsorbed layer at the ionic liquid/electrified metal interface. *J. Phys. Chem. B* **2010**, *114*, 8453−8459.
(23) Merlet, C.; Salanne, M.; Rotenberg, B.; Madden, P. A. Imidazolium ionic liquid interfaces with vapor and graphite: interfacial tension and capacitance from coarse-grained molecular simulations. *J. Phys. Chem. C* **2011**, *115*, 16613−16618.
(24) Merlet, C.; Rotenberg, B.; Madden, P. A.; Salanne, M. Computer simulations of ionic liquids at electrochemical interfaces. *Phys. Chem. Chem. Phys.* **2013**, *15*, 15781−15792.
(25) Pean, C.; Daffos, B.; Merlet, C.; Rotenberg, B.; Taberna, P.-L.; Simon, P.; Salanne, M. Single electrode capacitances of porous carbons in neat ionic liquid electrolyte at 100 C: a combined experimental and modeling approach. *J. Electrochem. Soc.* **2015**, *162*, A5091−A5095.
(26) Rupp, B.; Schmuck, M.; Balducci, A.; Winter, M.; Kern, W. Polymer electrolyte for lithium batteries based on photochemically crosslinked poly(ethylene oxide) and ionic liquid. *Eur. Polym. J.* **2008**, *44*, 2986−2990.
(27) Lux, S. F.; Schmuck, M.; Appetecchi, G. B.; Passerini, S.; Winter, M.; Balducci, A. Lithium insertion in graphite from ternary ionic liquid-lithium salt electrolytes: II. Evaluation of specific capacity and cycling efficiency and stability at room temperature. *J. Power Sources* **2009**, *192*, 606−611.
(28) Lux, S. F.; Schmuck, M.; Jeong, S.; Passerini, S.; Winter, M.; Balducci, A. Li-ion anodes in air-stable and hydrophobic ionic liquid-based electrolyte for safer and greener batteries. *Int. J. Energy Res.* **2010**, *34*, 97−106.
(29) Vogl, T.; Menne, S.; Kühnel, R.-S.; Balducci, A. The beneficial effect of protic ionic liquids on the lithium environment in electrolytes for battery applications. *J. Mater. Chem. A* **2014**, *2*, 8258−8265.
(30) Kirchner, B.; Hollóczki, O.; Canongia Lopes, J. N.; Pádua, A. A. H. Multiresolution calculation of ionic liquids. *Wiley Interdiscip. Rev.: Comput. Mol. Sci.* **2014**, 202−214.
(31) Niedermeyer, H.; Hallett, J. P.; Villar-Garcia, I. J.; Hunt, P. A.; Welton, T. Mixtures of ionic liquids. *Chem. Soc. Rev.* **2012**, *41*, 7780.
(32) Brüssel, M.; Brehm, M.; Pensado, A. S.; Malberg, F.; Ramzan, M.; Stark, A.; Kirchner, B. On the ideality of binary mixtures of ionic liquids. *Phys. Chem. Chem. Phys.* **2012**, *14*, 13204.
(33) Brehm, M.; Weber, H.; Pensado, A. S.; Stark, A.; Kirchner, B. Proton transfer and polarity changes in ionic liquid-water mixtures: a perspective on hydrogen bonds from ab initio molecular dynamics at the example of 1-ethyl-3-methylimidazolium acetate-water mixtures—Part 1. *Phys. Chem. Chem. Phys.* **2012**, *14*, 5030.
(34) Seddon, K. R.; Stark, A.; Torres, M.-J. Influence of chloride, water, and organic solvents on the physical properties of ionic liquids. *Pure Appl. Chem.* **2000**, *72*, 2275−2287.
(35) Sharma, A.; Ghorai, P. K. Effect of water on structure and dynamics of [BMIM][PF6] ionic liquid: An all-atom molecular dynamics simulation investigation. *J. Chem. Phys.* **2016**, *144*, No. 114505.
(36) Amigues, E.; Hardacre, C.; Keane, G.; Migaud, M.; O'Neill, M. Ionic liquids—media for unique phosphorus chemistry. *Chem. Commun.* **2006**, 72−74.
(37) Anthony, J. L.; Maginn, E. J.; Brennecke, J. F. Solution thermodynamics of imidazolium-based ionic liquids and water. *J. Phys. Chem. B* **2001**, *105*, 10942−10949.
(38) Jacquemin, J.; Husson, P.; Pádua, A. A.; Majer, V. Density and viscosity of several pure and water-saturated ionic liquids. *Green Chem.* **2006**, *8*, 172−180.
(39) Kelkar, M. S.; Maginn, E. J. Effect of temperature and water content on the shear viscosity of the ionic liquid 1-ethyl-3-methylimidazolium bis(trifluoromethanesulfonyl)imide as studied by atomistic simulations. *J. Phys. Chem. B* **2007**, *111*, 4867−4876.
(40) Deschamps, J.; Costa Gomes, M. F.; Pádua, A. A. Molecular simulation study of interactions of carbon dioxide and water with ionic liquids. *ChemPhysChem* **2004**, *5*, 1049−1052.
(41) Nockemann, P.; Binnemans, K.; Thijs, B.; Parac-Vogt, T. N.; Merz, K.; Mudring, A.-V.; Menon, P. C.; Rajesh, R. N.; Cordoyiannis, G.; Thoen, J.; Leys, J.; Glorieux, C. Temperature-Driven Mixing-Demixing Behavior of Binary Mixtures of the Ionic Liquid Choline Bis(trifluoromethylsulfonyl)imide and Water. *J. Phys. Chem. B* **2009**, *113*, 1429−1437.

DOI: 10.1021/acsomega.8b00995
ACS Omega 2018, 3, 8567−8582

(42) Wang, H.; Gurau, G.; Kelley, S. P.; Myerson, A. S.; Rogers, R. D. Hydrophobic vs. hydrophilic ionic liquid separations strategies in support of continuous pharmaceutical manufacturing. *RSC Adv.* **2013**, *3*, 10019−10026.
(43) Kohno, Y.; Ohno, H. Ionic liquid/water mixtures: from hostility to conciliation. *Chem. Commun.* **2012**, *48*, 7119−7130.
(44) Canongia Lopes, J. N.; Costa Gomes, M. F.; Pádua, A. A. Nonpolar, polar, and associating solutes in ionic liquids. *J. Phys. Chem. B* **2006**, *110*, 16816−16818.
(45) Schröder, C.; Rudas, T.; Neumayr, G.; Benkner, S.; Steinhauser, O. On the collective network of ionic liquid/water mixtures. I. Orientational structure. *J. Chem. Phys.* **2007**, *127*, No. 234503.
(46) Annapureddy, H. V.; Hu, Z.; Xia, J.; Margulis, C. J. How does water affect the dynamics of the room-temperature ionic liquid 1-hexyl-3-methylimidazolium hexafluorophosphate and the fluorescence spectroscopy of coumarin-153 when dissolved in it? *J. Phys. Chem. B* **2008**, *112*, 1770−1776.
(47) Spickermann, C.; Thar, J.; Lehmann, S.; Zahn, S.; Hunger, J.; Buchner, R.; Hunt, P.; Welton, T.; Kirchner, B. Why are ionic liquid ions mainly associated in water? A Car-Parrinello study of 1-ethyl-3-methyl-imidazolium chloride water mixture. *J. Chem. Phys.* **2008**, *129*, No. 104505.
(48) Bernardes, C. E.; Minas da Piedade, M. E.; Canongia Lopes, J. N. The structure of aqueous solutions of a hydrophilic ionic liquid: The full concentration range of 1-ethyl-3-methylimidazolium ethylsulfate and water. *J. Phys. Chem. B* **2011**, *115*, 2067−2074.
(49) Ab Rani, M. A.; Brant, A.; Crowhurst, L.; Dolan, A.; Lui, M.; Hassan, N. H.; Hallett, J. P.; Hunt, P. A.; Niedermeyer, H.; Perez-Arlandis, J. M.; Schrems, M.; Welton, T.; Wilding, R. Understanding the polarity of ionic liquids. *Phys. Chem. Chem. Phys.* **2011**, *13*, 16831−16840.
(50) Niedermeyer, H.; Hallett, J. P.; Villar-Garcia, I. J.; Hunt, P. A.; Welton, T. Mixtures of ionic liquids. *Chem. Soc. Rev.* **2012**, *41*, 7780−7802.
(51) Feng, S.; Voth, G. A. Molecular dynamics simulations of imidazolium-based ionic liquid/water mixtures: alkyl side chain length and anion effects. *Fluid Phase Equilib.* **2010**, *294*, 148−156.
(52) Baldelli, S. Influence of water on the orientation of cations at the surface of a room-temperature ionic liquid: A sum frequency generation vibrational spectroscopic study. *J. Phys. Chem. B* **2003**, *107*, 6148−6152.
(53) Rivera-Rubero, S.; Baldelli, S. Influence of water on the surface of hydrophilic and hydrophobic room-temperature ionic liquids. *J. Am. Chem. Soc.* **2004**, *126*, 11788−11789.
(54) Bowers, J.; Butts, C. P.; Martin, P. J.; Vergara-Gutierrez, M. C.; Heenan, R. K. Aggregation behavior of aqueous solutions of ionic liquids. *Langmuir* **2004**, *20*, 2191−2198.
(55) Consorti, C. S.; Suarez, P. A.; de Souza, R. F.; Burrow, R. A.; Farrar, D. H.; Lough, A. J.; Loh, W.; da Silva, L. H.; Dupont, J. Identification of 1,3-dialkylimidazolium salt supramolecular aggregates in solution. *J. Phys. Chem. B* **2005**, *109*, 4341−4349.
(56) Moreno, M.; Castiglione, F.; Mele, A.; Pasqui, C.; Raos, G. Interaction of Water with the Model Ionic Liquid [bmim][BF4]: Molecular Dynamics Simulations and Comparison with NMR Data. *J. Phys. Chem. B* **2008**, *112*, 7826−7836.
(57) Fazio, B.; Triolo, A.; Di Marco, G. Local organization of water and its effect on the structural heterogeneities in room-temperature ionic liquid/H_2O mixtures. *J. Raman Spectrosc.* **2008**, *39*, 233−237.
(58) Gehrke, S.; Hollóczki, O. Are There Carbenes in N-Heterocyclic Carbene Organocatalysis? *Angew. Chem., Int. Ed.* **2017**, *56*, 16395−16398.
(59) Gehrke, S.; Hollóczki, O. Treten in der N-heterozyklischen Carben-Organokatalyse wirklich Carbene auf? *Angew. Chem.* **2017**, *129*, 16613−16617.
(60) D'Angelo, P.; Serva, A.; Aquilanti, G.; Pascarelli, S.; Migliorati, V. Structural Properties and Aggregation Behavior of 1-Hexyl-3-methylimidazolium Iodide in Aqueous Solutions. *J. Phys. Chem. B* **2015**, *119*, 14515−14526.
(61) Serva, A.; Migliorati, V.; Lapi, A.; Aquilanti, G.; Arcovito, A.; D'Angelo, P. Structural properties of geminal dicationic ionic liquid/water mixtures: a theoretical and experimental insight. *Phys. Chem. Chem. Phys.* **2016**, *18*, 16544−16554.
(62) Köddermann, T.; Wertz, C.; Heintz, A.; Ludwig, R. The association of water in ionic liquids: a reliable measure of polarity. *Angew. Chem., Int. Ed.* **2006**, *45*, 3697−3702.
(63) Köddermann, T.; Wertz, C.; Heintz, A.; Ludwig, R. Ion-Pair Formation in the Ionic Liquid 1-Ethyl-3-methylimidazolium Bis-(triflyl)imide as a Function of Temperature and Concentration. *ChemPhysChem* **2006**, *7*, 1944−1949.
(64) Köddermann, T.; Paschek, D.; Ludwig, R. Molecular dynamic simulations of ionic liquids: A reliable description of structure, thermodynamics and dynamics. *ChemPhysChem* **2007**, *8*, 2464−2470.
(65) Fumino, K.; Wulf, A.; Ludwig, R. The Cation−Anion Interaction in Ionic Liquids Probed by Far-Infrared Spectroscopy. *Angew. Chem., Int. Ed.* **2008**, *47*, 3830−3834.
(66) Fumino, K.; Wulf, A.; Ludwig, R. Strong, localized, and directional hydrogen bonds fluidize ionic liquids. *Angew. Chem., Int. Ed.* **2008**, *47*, 8731−8734.
(67) Fumino, K.; Wulf, A.; Ludwig, R. Hydrogen bonding in protic ionic liquids: reminiscent of water. *Angew. Chem., Int. Ed.* **2009**, *48*, 3184−3186.
(68) Fumino, K.; Wulf, A.; Ludwig, R. The potential role of hydrogen bonding in aprotic and protic ionic liquids. *Phys. Chem. Chem. Phys.* **2009**, *11*, 8790−8794.
(69) Wulf, A.; Fumino, K.; Ludwig, R. Spectroscopic evidence for an enhanced anion-cation interaction from hydrogen bonding in pure imidazolium ionic liquids. *Angew. Chem., Int. Ed.* **2010**, *49*, 449−453.
(70) Stange, P.; Fumino, K.; Ludwig, R. Ion Speciation of Protic Ionic Liquids in Water: Transition from Contact to Solvent-Separated Ion Pairs. *Angew. Chem., Int. Ed.* **2013**, *52*, 2990−2994.
(71) Bier, M.; Mars, J.; Li, H.; Mezger, M. Salt-induced micro-heterogeneities in binary liquid mixtures. *Phys. Rev. E* **2017**, *96*, No. 022603.
(72) Martínez, L.; Andrade, R.; Birgin, E. G.; Martínez, J. M. A package for building initial configurations for molecular dynamics simulations. *J. Comput. Chem.* **2009**, *30*, 2157−2164.
(73) CP2k, A General Program to Perform Molecular Dynamics Simulations. CP2k Developers Group under the Terms of the GNU General Public License. http://cp2k.berlios.de/.
(74) VandeVondele, J.; Krack, M.; Mohamed, F.; Parrinello, M.; Chassaing, T.; Hutter, J. QUICKSTEP: Fast and Accurate Density Functional Calculations Using a Mixed Gaussian and Plane Waves Approach. *Comput. Phys. Commun.* **2005**, *167*, 103−128.
(75) VandeVondele, J.; Hutter, J. Gaussian Basis Sets for Accurate Calculations on Molecular Systems in Gas and Condensed Phases. *J. Chem. Phys.* **2007**, *127*, No. 114105.
(76) Goedecker, S.; Teter, M.; Hutter, J. Separable Dual-Space Gaussian Pseudopotentials. *Phys. Rev. B* **1996**, *54*, 1703−1710.
(77) Hartwigsen, C.; Goedecker, S.; Hutter, J. Relativistic Separable Dual-Space Gaussian Pseudopotentials from H to Rn. *Phys. Rev. B* **1998**, *58*, 3641−3662.
(78) Krack, M. Pseudopotentials for H to Kr Optimized for Gradient-Corrected Exchange-Correlation Functionals. *Theor. Chem. Acc.* **2005**, *114*, 145−152.
(79) Grimme, S.; Antony, J.; Ehrlich, S.; Krieg, H. A consistent and accurate ab initio parametrization of density functional dispersion correction (DFT-D) for the 94 elements H-Pu. *J. Chem. Phys.* **2010**, *132*, No. 154104.
(80) Grimme, S.; Ehrlich, S.; Goerigk, L. Effect of the damping function in dispersion corrected density functional theory. *J. Comput. Chem.* **2011**, *32*, 1456−1465.
(81) Blöchl, P. E. Electrostatic decoupling of periodic images of plane wave expanded densities and derived atomic point charges. *J. Chem. Phys.* **1995**, *103*, 7422−7428.
(82) Mulliken, R. S. Electronic Population Analysis on LCAO-MO Molecular Wave Functions. I. *J. Chem. Phys.* **1955**, *23*, 1833−1840.

DOI: 10.1021/acsomega.8b00995
ACS Omega 2018, 3, 8567−8582

(83) Brehm, M.; Kirchner, B. TRAVIS - A Free Analyzer and Visualizer for Monte Carlo and Molecular Dynamics Trajectories. *J. Chem. Inf. Model.* **2011**, *51*, 2007−2023.
(84) GRACE. http://plasma-gate.weizmann.ac.il/Grace/, http://plasma-gate.weizmann.ac.il/Grace/.
(85) Gnuplot developers group. http://www.gnuplot.info/.
(86) Brehm, M.; Weber, H.; Thomas, M.; Hollóczki, O.; Kirchner, B. Domain Analysis in Nanostructured Liquids: A Post-Molecular Dynamics Study at the Example of Ionic Liquids. *ChemPhysChem* **2015**, *16*, 3271−3277.
(87) Hollóczki, O.; Macchiagodena, M.; Weber, H.; Thomas, M.; Brehm, M.; Stark, A.; Russina, O.; Triolo, A.; Kirchner, B. Triphilic Ionic-Liquid Mixtures: Fluorinated and Non-fluorinated Aprotic Ionic-Liquid Mixtures. *ChemPhysChem* **2015**, *16*, 3325−3333.
(88) Freire, M. G.; Neves, C. M. S. S.; Marrucho, I. M.; Coutinho, J. A. P.; Fernandes, A. M. Hydrolysis of Tetrafluoroborate and Hexafluorophosphate Counter Ions in Imidazolium-Based Ionic Liquids. *J. Phys. Chem. A* **2010**, *114*, 3744−3749.
(89) Wendler, K.; Thar, J.; Zahn, S.; Kirchner, B. Estimating the Hydrogen Bond Energy. *J. Phys. Chem. A* **2010**, *114*, 9529−9536.
(90) Elfgen, R.; Hollóczki, O.; Kirchner, B. A Molecular Level Understanding of Template Effects in Ionic Liquids. *Acc. Chem. Res.* **2017**, *50*, 2949−2957.
(91) Mele, A.; Romanò, G.; Giannone, M.; Ragg, E.; Fronza, G.; Raos, G.; Marcon, V. The Local Structure of Ionic Liquids: Cation-Cation NOE Interactions and Internuclear Distances in Neat [BMIM][BF_4] and [BDMIM][BF_4]. *Angew. Chem., Int. Ed.* **2006**, *45*, 1123−1126.
(92) Matthews, R. P.; Welton, T.; Hunt, P. A. Competitive pi interactions and hydrogen bonding within imidazolium ionic liquids. *Phys. Chem. Chem. Phys.* **2014**, *16*, 3238−3253.
(93) Weber, H.; Hollóczki, O.; Pensado, A. S.; Kirchner, B. Side chain fluorination and anion effect on the structure of 1-butyl-3-methylimidazolium ionic liquids. *J. Chem. Phys.* **2013**, *139*, No. 084502.
(94) Gehrke, S.; von Domaros, M.; Clark, R.; Holloczki, O.; Brehm, M.; Welton, T.; Luzar, A.; Kirchner, B. Structure and lifetimes in ionic liquids and their mixtures. *Faraday Discuss.* **2018**, *206*, 219−245.
(95) Rapaport, D. C. Hydrogen bonds in water. *Mol. Phys.* **1983**, *50*, 1151−1162.
(96) Luzar, A.; Chandler, D. Hydrogen-bond kinetics in liquid water. *Nature* **1996**, *379*, 55−57.
(97) Luzar, A.; Chandler, D. Effect of Environment on Hydrogen Bond Dynamics in Liquid Water. *Phys. Rev. Lett.* **1996**, *76*, 928−931.
(98) Pensado, A. S.; Brehm, M.; Thar, J.; Seitsonen, A. P.; Kirchner, B. Effect of Dispersion on the Structure and Dynamics of the Ionic Liquid 1-Ethyl-3-methylimidazolium Thiocyanate. *ChemPhysChem* **2012**, *13*, 1845−1853.
(99) Gabl, S.; Schroeder, C.; Steinhauser, O. Computational studies of ionic liquids: Size does matter and time too. *J. Chem. Phys.* **2012**, *137*, No. 094501.
(100) Sheridan, Q. R.; Schneider, W. F.; Maginn, E. J. Anion Dependent Dynamics and Water Solubility Explained by Hydrogen Bonding Interactions in Mixtures of Water and Aprotic Heterocyclic Anion Ionic Liquids. *J. Phys. Chem. B* **2016**, *120*, 12679−12686.
(101) Dommert, F.; Schmidt, J.; Krekeler, C.; Zhao, Y. Y.; Berger, R.; Site, L. D.; Holm, C. Towards multiscale modeling of ionic liquids: From electronic structure to bulk properties. *J. Mol. Liq.* **2010**, *152*, 2−8 Part of Molten Salts and Ionic Liquids Special issue of the EUCHEM − Conference, Kopenhagen, 2008.
(102) Lehmann, S. B. C.; Roatsch, M.; Schöppke, M.; Kirchner, B. On the physical origin of the cation-anion intermediate bond in ionic liquids Part I. Placing a (weak) hydrogen bond between two charges. *Phys. Chem. Chem. Phys.* **2010**, *12*, 7473−7486.

DOI: 10.1021/acsomega.8b00995
ACS Omega 2018, 3, 8567−8582